Acta Geologica Sinica (English Edition), 2019, 93(6): 1721–1737

Early Paleozoic Granite in the Talate Mining District, Chinese Altay, and its Geological Significance for the Altay Orogenic Belt

LIU Feng[1, *], CHAI Fengmei[2] and HAN Dan[1]

[1] *MNR Key Laboratory of Metallogeny and Mineral Assessment, Institute of Mineral Resources, Chinese Academy of Geological Sciences, Beijing 10037, China*
[2] *College of Geology & Prospecting Engineering Program, Xinjiang University, Urumqi 830046, China*

Abstract: Zircon dating, geochemical and Nd-Sr isotopic analyses have been determined for samples from two granitic intrusions in the Talate mining district, Chinese Altay. Our data suggest that these intrusions were emplaced from 462.5 Ma to 457.8 Ma. These rocks have strong affinity to peralumious S-type granite and are characterized by prominent negative Eu anomalies (δEu=0.20–0.35), strong depletion in Ba, Sr, P, Ti, Nb, Ta and positive anomalies in Rb, Th, U, K, La, Nd, Zr, Hf. Nd-Sr isotopic compositions of the whole rock show negative $\varepsilon_{Nd}(t)$ values (−1.21 to −0.08) and Mesoproterozoic Nd model ages (T_2^{DM}=1.20–1.30 Ga). Their precursor magmas were likely derived from the partial dehydration melting of Mesoproterozoic mica-rich pelitic sources and mixed with minor mantle-derived components, under relatively low P (≤1 kbar) and high T (746–796°C) conditions. A ridge subduction model may account for the early Paleozoic geodynamic process with mantle-derived magmas caused by Ordovician ridge subduction and the opening of a slab window underplated and/or intraplated in the middle–upper crust, which triggered extensive partial melting of the shallow crust to generate diverse igneous rocks, and provided the heat for the crustal melting and juvenile materials for crustal growth.

Key words: geochronology, geochemistry, S-type granite, ridge subduction, Chinese Altay, Xinjiang province

Citation: Liu et al., 2019. Early Paleozoic Granite in the Talate Mining District, Chinese Altay, and its Geological Significance for the Altay Orogenic Belt. Acta Geologica Sinica (English Edition), 93(6): 1721–1737. DOI: 10.1111/1755-6724.13819

1 Introduction

The Altay orogenic belt is an important component of the Central Asian Orogenic Belt (CAOB) (Jahn et al., 2000a, b) (Fig. 1a), which extends in a NW–SE direction for ~2000 km from Kazakhstan and Russia through northern Xinjiang to southwestern Mongolia. Some 500 km of the length of the CAOB is within China (Liu et al., 2010), where it contains several examples of large-scale Cu, Au, polymetallic, and rare-metal (Li, Be, Nb, and Ta) mineralization (Hong et al., 2003). The Altay orogenic belt is the key to understanding the development of accretionary orogeny in Central Asia (Wang et al., 2006). The mechanisms of formation and evolution of the CAOB have been extensively investigated (Buslov et al., 2002; Windley et al., 2002; Buslov et al., 2004; Safonova et al., 2004; Yuan et al., 2007; Sun et al., 2008; Uchio et al., 2008; Xiao et al., 2008, 2009). Some studies have revealed a complex accretionary evolution involving a collage of tectonostratigraphic terranes, including Precambrian continental blocks (e.g., Coleman, 1989; Mossakovsky et al., 1993; Badarch et al., 2002; Windley et al., 2002; Xiao et al., 2004; Windley et al., 2007; Wang et al., 2009). So, the study for the processes of magmatism during the different stages is imperative to understand such a complicated orogen.

The Chinese Altay is located close to the northern border of Xinjiang, separating China from Kazakhstan to the northwest, Russia to the north, and Mongolia to the northeast. The Chinese Altay is composed of different crustal terranes and is an ideal region in which to study Phanerozoic crustal growth and metallogenesis associated with the CAOB (Fig. 1b). Compared with the record of late Paleozoic magmatism, there have been far fewer reports of Ordovician granitic magmatismfor the early stages of development of the Chinese Altay. Examples of Ordovician rocks include small gneissic granitic stocks from the Jiadengyu area in the west (453, 466, and 479 Ma; Sun et al., 2008, 2009; Cai et al., 2011a), the Qiemuqiek batholith in the south (462 Ma; Wang et al., 2006), and the Tiemierte batholith in the north (459 Ma; Chai et al., 2010) of the region (Fig. 1b). The studies of geochemistry, geochronology, and zircon O or Hf isotopic compositions for the early–middle Paleozoic granites by Sun et al. (2009) and Cai et al. (2011a) proposed that these granites were formed in an arc setting related to ridge subduction and that the Chinese Altay might possibly represent a magmatic arc built on the southern margin of the Siberian Craton. However, Wang et al. (2006) and Chai et al. (2010) suggested that the early Paleozoic granites represent the magmatic arc of the margin of the Altay microcontinent.

This study presents the results of SHRIMP U–Pb dating

* Corresponding author. E-mail: liufeng@cags.ac.cn

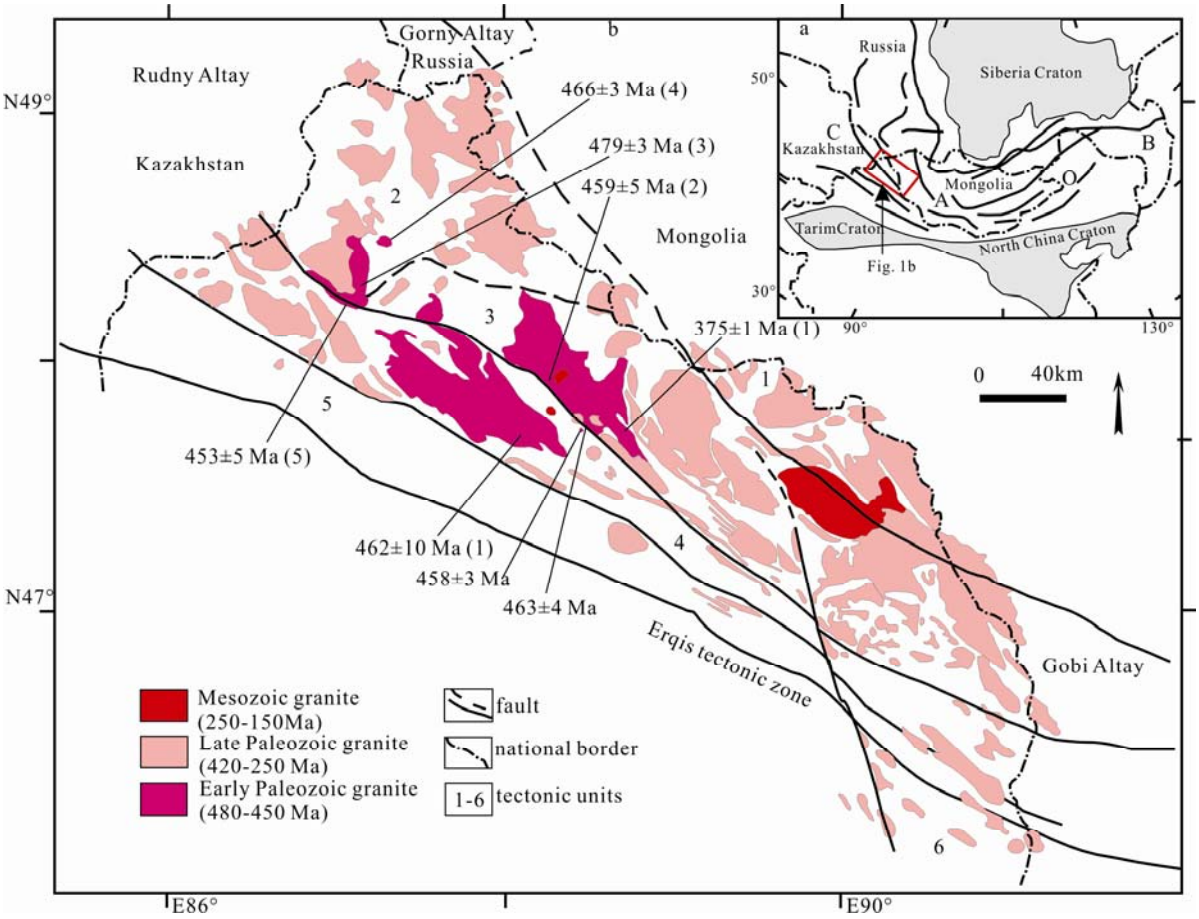

Fig. 1. (a) Simplified tectonics showing the extension of the CAOB (modified from Sun et al., 2008); (b) map showing the distribution of granitic rocks in the Chinese Altay (modified from Song et al., 2017 and references therein).
The red box in Fig. 1a represents the Chinese Altay; ages of Early Paleozoic granites in Fig. 1b are all zircon U–Pb dates from (1) Wang et al., 2006, (2) Chai et al., 2010, (3) Cai et al., 2011a, (4) Sun et al., 2009, and (5) Sun et al., 2008.

of zircons as well as geochemical and isotopic analyses of granites in the north of the Talate mining district, near the southern margin of the Altay, Xinjiang province, China. These data are used to constrain the petrogenesis of the rocks to better understand the processes of magmatism and the tectonic evolution of the Altay orogen during the Ordovician. Finally, support is provided for existing models regarding the early stages of subduction and accretion in the Altay orogen.

2 Regional Geology

The Chinese Altay is situated between the southern margin of the Siberian plate and the northern margin of the Kazakhstan–Junggar plate (Chai et al., 2009). It is bounded to the northwest by the Rudny Altay of Kazakhstan and the Gorny Altay of Russia, to the southeast by the Gobi Altay of Mongolia, and to the south by the Erqis Fault (Fig. 1b). The Chinese Altay includes three main terranes, namely, the North Altay (including two terranes: northern and central) and the South Altay (Li et al., 2003; He et al., 2004; Zhu et al., 2006; Chai et al., 2009) (Fig. 2a), as well as being subdivided into six units from 1 to 6 (Fig. 1b) (Wang et al., 2009). From north to south, Unit 1 is included within the Northern Altay, Units 2 and 3 belong to the Central Altay, and Units 4, 5 and 6 are part of the South Altay. The units are fault-bounded blocks separated by several NW–SE-trending deep faults that are roughly parallel to the major Erqis Fault in the south. Together, the terranes define an island-arc subduction zone with ages that young southward (Xiao et al., 2008; Wang et al., 2009).

The Northern Altay, or Unit 1, consists predominantly of Devonian to Carboniferous volcanosedimentary sequences, including middle to late Devonian andesites and dacites and late Devonian to early Carboniferous sedimentary rocks (e.g., shale, sandstone, and limestone). These sedimentary sequences, which formed in an island-arc setting (Xiao et al., 2004), are intruded by Carboniferous to Permian granitoids (Li et al., 2003). Minor Jurassic granites are also exposed in the area (Yuan et al., 2001).

Units 2 and 3 constitute the Central Altay (Windley et al., 2002; Xiao et al., 2004; Wang et al., 2009). Unit 2 is composed mainly of the Neoproterozoic to middle Ordovician Habahe Group, which includes low-grade metamorphosed volcanosedimentary rocks that are unconformably overlain by limestone and sandstone,

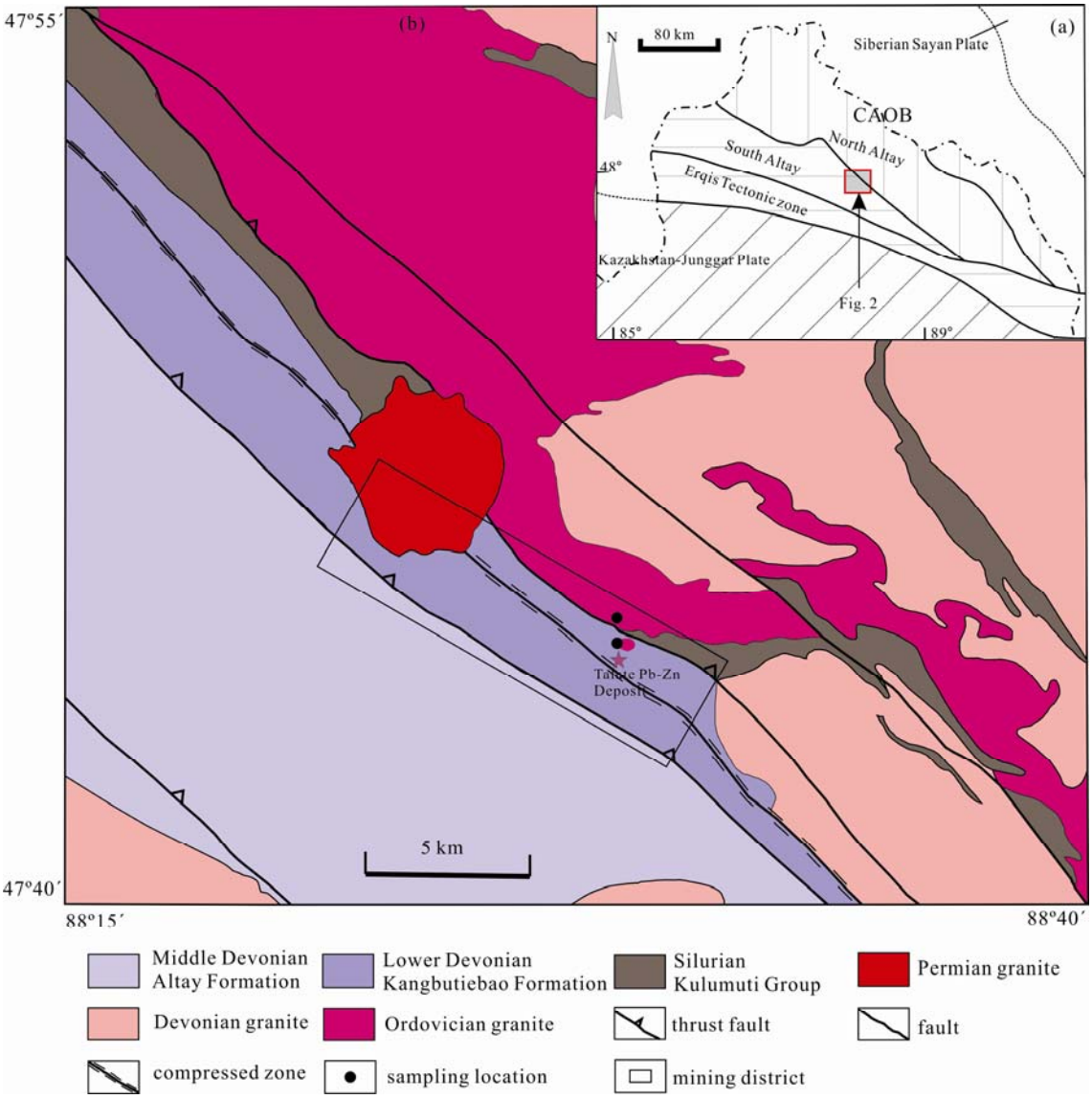

Fig. 2. (a) Tectonic map showing the main terranes in the Chinese Altay (from He et al., 2004); (b) simplified geological map showing the main strata, granotoids and tectonics in and around the Talate mining district.

along with minor early Devonian volcanosedimentary rocks. Unit 3 contains amphibolite- and greenschist-facies metasedimentary and metavolcanic rocks (Wang et al., 2009). Intrusive magmatism in the Central Altay is widespread and consists mainly of Ordovician to early Devonian synorogenic I- or S- type granites with some mafic plutons (e.g., Li et al., 2003; Wang et al., 2006; Yuan et al., 2007; Liu et al., 2008; Sun et al., 2008, 2009; Chai et al., 2010; Cai et al., 2011a). Recently, granitic plutons of Triassic age have also been identified in the area, including the Alaer granitic batholith (Wang et al., 2009; Liu et al., 2014). The Central Altay is considered to be the most important part of the Altay microcontinent (Hu et al., 2000; Li et al., 2003; Xiao et al., 2004; Wang et al., 2009). The fault-bounded southern border of the pluton studied here marks the boundary between the Central Altay and the South Altay. In the South Altay, the strata include low-grade metamorphosed rocks of the Neoproterozoic tomiddle Ordovician Habahe Group, low-grade metamorphosed volcanic and marine sedimentary rocks of the late Silurian to early Devonian Kangbutiebao Formation, and the middle Devonian Altay Formation, which consists of sedimentary rocks intercalated with low-grade bimodal metavolcanic rocks. Ordovician volcanic rocks and sedimentary clastic rocks of the Silurian Kulumuti Group are less commonly exposed in the South Altay. However, the area contains voluminous Paleozoic (mainly early Devonian, as well as late Carboniferous to Permian and minor Ordovician) synorogenic and post-collisional granitoids (Tong et al., 2005, 2006, 2007; Wang et al., 2006, 2007; Yuan et al., 2007).

Four NW-trending fault-bounded volcanosedimentary basins (the Kelang, Maizi, Chonghuer, and Ashile basins) form part of Unit 4. The Kangbutiebao and Altay formations crop out in the Kelang, Maizi, and Chonghuer basins, and the Ashile Formation occurs within the Ashile

Basin. Rocks in the four basins underwent regional greenschist to lower-amphibolite facies metamorphism, and substantial Fe, Cu, and Pb–Zn polymetallic deposits are hosted within their volcanic strata (Chai et al., 2009). Unit 5 is composed mainly of fossiliferous Devonian sediments overlain by late Carboniferous sedimentary rocks. Older gneisses and schists occur locally. Unit 6 consists primarily of Devonian rocks with an island-arc affinity (Mei et al., 1993; Yu et al., 1993; Wang et al., 2009).

The Kelang Basin is located between the Bazhai and Kezijiaer faults. The main exposed strata include those of the Kulumuti Group, which are distributed locally along the margin of the Basin, and those of the Kangbutiebao and Altay formations. The lower part of the Kangbutiebao Formation sits unconformably on the Silurian Kulumuti Group and is conformably overlain by rocks of the Altay Formation (Chai et al., 2009). The Talate Pb–Zn and Fe deposit is situated in the southeast of the Basin. Two granitic plutons crop out in the mineralized area. One is the Permian Lamazhao granite stock, located in the northwest of the mining district (Wang et al., 2005). The other is a large batholith to the north of the Talate deposit (Fig. 2b), which is a late Paleozoic granite, according to the 1:200,000 geological map of the area (Xinjiang Bureau of Geology and Mineral Resources, 1978), and is considered to have formed at either 375 Ma (TIMS U–Pb age of a single zircon, Wang et al., 2006) or 344 Ma (Rb–Sr whole-rock age; Zhang et al., 1996). This study will focus on this granitic batholith in the Central Altay.

3 Field Relationships and Petrography

The main body of granite is located in the Central Altay. Its southern marginal facies crop out locally in the north of the Talate mining district. The batholith crops out over an area of >100 km^2 and extends as a NW-trending regional belt that is separated from rocks to the south by a regional fault. The granitic rocks within the batholith comprise biotite granite, biotite–plagioclase granite, muscovite–plagioclase granite and two-mica syenogranite.

The southern margin of the batholith,where we collected samples, is composed of two-mica syenogranite (Fig. 3b) with a variably developed gneissose structure. The rocks are gray and medium to fine grained. In thin section (Fig. 3a), the granite is composed mainly of K-feldspar (45%–50%), plagioclase (~25%), quartz (~20%), muscovite (~5%%), biotite (~5%)and local cordierite. Accessory minerals are mostlymagnetite, zirconand apatite; minor sericite is interpreted to be secondary. K-feldsparis 2–5 mm across and forms predominantly anhedral to subhedral crystals that exhibit partial fragmentation and recrystallization. Plagioclase (1–3 mm) occurs mostly as subhedral (but rarely anhedral) crystals that exhibit local minor sericitization and the bending of twinning planes. Quartz occurs as anhedral grains 0.4–5 mm in diameter and as aggregates spatially associated with feldspar. Quartz grains are commonly slightly elongated, show a weak preferred orientation, and exhibit undulose extinction. Muscovite and biotite occur as grain aggregates that define a weak preferred orientation.

A small (<0.25 km^2) granite stock, where othersamples were collected,islocated in rocks of the Kangbutiebao Formation. The granite is petrographically similar to rocks of the main batholith and comprises ~50% K-feldspar, ~20% plagioclase, ~20% quartz, ~10% mica (both muscovite and biotite) and minor cordierite.K-feldspar (5–10 mm) occurs predominantly as anhedral to subhedral crystals containing small quantities of poikilitic plagioclase sometimes,but also as recrystallized grain aggregates. Plagioclase (0.2–3 mm) occurs as subhedral to anhedral crystals, locally exhibiting recrystallization and/or minor sericitization. Single crystals or aggregates of quartz show undulose extinction. Biotite shows minor chloritization.

4 Sampling and Analytical Methods

SHRIMP U–Pb zircon dating was undertaken on zircon grains from two samples of mica-bearing syenogranite from the southern margin of the batholith and a small granite stock that is located in volcanic rocks in the Kangbutiebao Formation. In addition, seven representative and fresh whole-rock samples from the margin of the

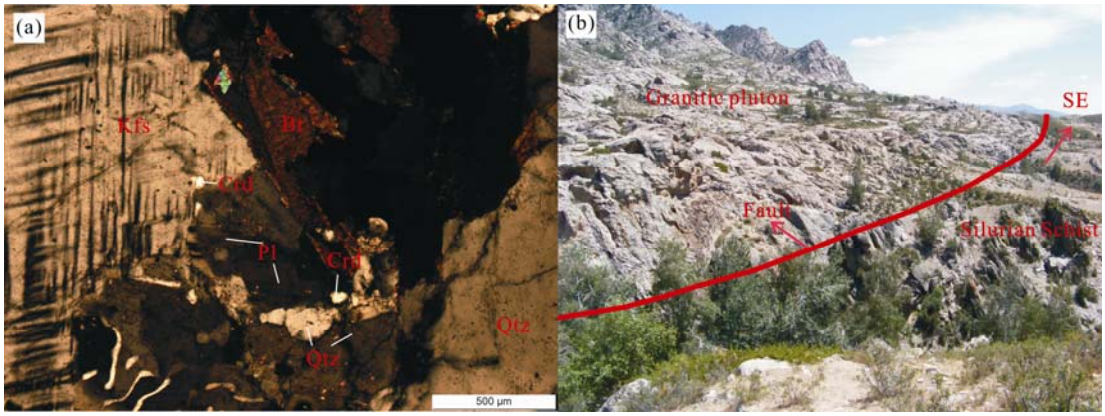

Fig. 3. Microscopic and field photographs of the two-mica syenogranite showing (a) K-feldspar as alattice twin under crossed polars, and (b) the pluton in the southern margin is separated from Silurian schist by a NW-trending regional fault.Kfs- K-feldspar, Pl-Plagioclase, Qtz-Quartz, Bt-Biotite, Crd-Cordierite.

batholith within about 1.5 km length and two samples from the stockwere analyzed to establish their geochemical and Sr–Nd isotopic compositions.

Zircon grains were separated from about 10 kg of each of the two samples by crushing followed by heavy liquid and magnetic separation, and then were cleaned in cold HF and HNO_3. Zircon grains were hand-picked under a microscope then mounted in epoxy and polished to half-thickness sections to expose their interiors. Each mount was imaged using a scanning electron microscope in backscattered electron and cathodoluminescence mode to characterize the internal morphologies of grains and to guide subsequent SHRIMP analysis spots. The zircon U–Pb analyses were conducted using the SHRIMP II ion microprobe at the Beijing SHRIMP Center, Chinese Academy of Geological Sciences, Ministry of Land and Resource of the People's Republic of China. Details of the analytical procedures followed are given in Williams and Claessin (1987). The debugging instrument and the specific methods of analysis are detailed in Song et al. (2002) and Zhu and Song (2006). During the SHRIMP determinations, the reference zircon TEM (417 Ma) was used to correct for isotopic fractionation, and standard 91500 (1062.4 Ma) was used to determine the U, Th and Pb isotopic concentrations of the samples. The common Pb component was corrected using the measured quantity of ^{204}Pb. The reproducibility of the two reference standards was measured at ca. 3%. The Concordia ages, uncertainties, mean square weighted deviations (MSWDs), and probabilities of fit were calculated using the Isoplot/Ex software (Ludwig, 2001). Uncertainties in individual analyses are quoted at the 1σ level based on counting statistics. The final Concordia age for each sample is given as the weighted mean of pooled $^{206}Pb/^{238}U$ ages at the 95% confidence level.

Major-element contents, rare-earth-element (REE) concentrations, and other trace-element concentrations were analyzed at the National Research Center for Geoanalysis, Chinese Academy of Geological Sciences (CAGS), Beijing. Absolute concentrations and isotopic ratios of Rb, Sr, Sm, and Nd were analyzed at the Isotope Laboratory of Institute of Geology, CAGS, Beijing. Major-element compositions were analyzed by X-ray fluorescence spectrometer (XRF-2100) using the Chinese national standard GB/T14506.28-1993 for calibration. Analytical errors are generally less than 2%. ICP–MASS (X-series) and ICP–AES (IRIS) were employed for the measurement of REE and other trace-element concentrations, using standards JY/T015-1996 and DZ/T0223-2001 for calibration, respectively. The precision of the measured concentrations is estimated to be 5%, and the accuracy is better than 5%. An isotope dilution method was used for the analysis of Rb, Sr, Sm, and Nd. Their concentrations and Sr isotopic compositions were measured using a Finnigan MAT262 multi-collector thermal ionization mass spectrometer, using $^{88}Sr/^{86}Sr=8.37521$ to correct for isotopic mass-dependent fractionation. Nd isotopic compositions were measured using a Nu Plasma HR MC–ICP–MS and DSN-100, using $^{146}Nd/^{144}Nd=0.7219$ for calibration purposes.

5 Results

5.1 Geochronology

The analyzed zircon grains from the granitic batholith are mostly colorless or light brown, and either transparent or translucent. Some grains are fractured, some slightly rounded, and some show minor alteration. Inclusions of opaque minerals are common. The majority of zircon grains are euhedral stubby prisms 70–120 μm in length and have aspect ratios of 1:1 to 2:1. In comparison, zircons grains from the granite stock are mostly light brownish yellow, translucent, moderately altered, andlarger (100–200 μm long), with aspect ratios of 2:1 to 3:1. In the CL images (Fig. 4a, b), all zircon grains show typical magmatic features such as apparently symmetrical or oscillatory zoning. Some grains have rounded cores and rims with well-developed oscillatory zoning, suggesting that the cores might be inherited components upon which magmatic rims grew subsequently. Some grains show relatively CL-bright homogenous rims, indicating recrystallization or metamictization resulting from post-magmatic hydrothermal activity (Du et al., 2005; Wang et al., 2007).

Zircons with well-developed oscillatory zoning and few inclusions and lacking CL-bright rims or fractures were chosen for dating. From each sample, 16 zircon grains were selected for analysis. In addition, a grain from each sample with an inherited core and a magmatic rim were analyzed, making a total of 17 analytical spots for each sample. The results are presented in Table 1.

The U and Th concentrations of zircon grains from the batholith range from 220 to 1725 ppm and from 104 to 603 ppm, respectively. The Th/U ratios range from 0.20 to

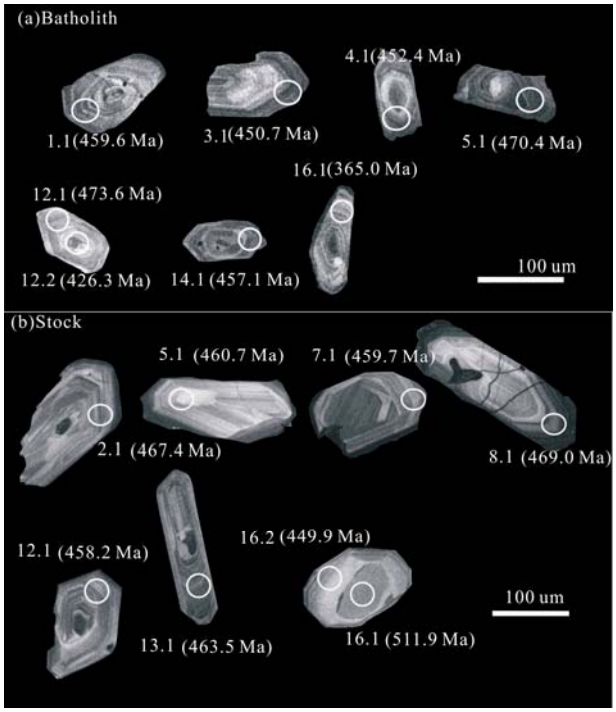

Fig. 4. CL images of zircons from the granitic batholith (a) and stock (b).
Analyzed spots are circled. Numbers in brackets are $^{206}Pb/^{238}U$ ages.

Table 1 SHRIMP zircon U-Pb dating results of two granites in the Talate mining district

Spot	U (ppm)	Th (ppm)	$^{232}Th/^{238}U$	$^{206}Pb^*$ (ppm)	$^{206}Pb_c$ %	$^{206}Pb^*/^{238}U$	±%	$^{207}Pb^*/^{235}U$	±%	$^{207}Pb^*/^{206}Pb^*$	±%	$^{206}Pb/^{238}U$ Age (Ma)	±1σ
Batholith													
1.1	523	194	0.38	33.3	0.15	0.074	1.3	0.57	1.9	0.056	1.4	459.6	5.9
2.1	510	138	0.28	32.4	0.24	0.074	1.3	0.57	2.3	0.056	1.9	459.0	5.8
3.1	220	104	0.49	13.7	0.32	0.072	1.6	0.59	3.8	0.059	3.4	450.7	7.0
4.1	362	114	0.33	22.7	0.13	0.073	1.3	0.56	2.1	0.056	1.6	452.4	5.8
5.1	1725	340	0.20	112.3	0.12	0.076	1.2	0.58	1.5	0.056	0.8	470.4	5.6
6.1	955	229	0.25	63.1	0.12	0.077	1.3	0.59	1.7	0.056	1.1	477.2	5.8
7.1	788	378	0.50	50.6	0.15	0.075	1.3	0.57	1.8	0.055	1.3	464.5	5.7
8.1	804	603	0.77	49.2	0.13	0.071	1.3	0.56	1.7	0.057	1.1	442.5	5.5
9.1	604	437	0.75	37.1	0.68	0.071	1.3	0.58	3.1	0.060	2.8	442.1	5.6
10.1	345	228	0.68	22.6	0.36	0.076	1.4	0.57	2.6	0.055	2.2	471.6	6.2
11.1	380	112	0.30	24.7	0.22	0.076	1.5	0.58	2.8	0.056	2.4	469.4	6.8
12.1	561	173	0.32	38.0	3.27	0.076	1.3	0.61	6.7	0.058	6.6	473.6	6.2
12.2	439	219	0.52	25.8	0.17	0.068	1.3	0.53	2.0	0.056	1.5	426.3	5.5
13.1	805	205	0.26	51.5	0.10	0.074	1.3	0.57	1.7	0.056	1.2	462.1	5.7
14.1	635	324	0.53	40.1	0.10	0.074	1.4	0.57	1.9	0.056	1.2	457.1	6.2
15.1	869	488	0.58	56.6	0.22	0.076	1.4	0.61	2.2	0.058	1.7	469.8	6.3
16.1	340	161	0.49	17.1	0.40	0.058	1.4	0.51	2.6	0.063	2.2	365.0	4.8
Stock													
1.1	295	147	0.52	19.2	0.45	0.075	1.4	0.58	3.3	0.056	3.0	468.7	6.2
2.1	335	161	0.50	21.7	0.19	0.075	1.3	0.58	2.1	0.056	1.6	467.4	6.0
3.1	154	155	1.04	9.9	0.47	0.075	1.8	0.56	4.2	0.055	3.8	463.6	8.3
4.1	75	71	0.98	4.6	0.72	0.071	1.8	0.56	5.7	0.057	5.4	444.8	7.9
5.1	313	202	0.67	19.9	0.00	0.074	1.4	0.58	2.5	0.057	2.1	460.7	6.0
6.1	132	86	0.67	8.3	0.66	0.072	1.5	0.55	6.7	0.055	6.5	449.8	6.7
7.1	348	206	0.61	22.3	0.68	0.074	1.3	0.57	3.1	0.056	2.8	459.7	6.0
8.1	448	122	0.28	29.1	0.15	0.076	1.5	0.59	2.1	0.057	1.4	469.0	6.9
9.1	74	50	0.70	4.6	1.33	0.072	1.7	0.53	5.0	0.053	4.7	447.8	7.5
10.1	254	130	0.53	16.0	0.31	0.073	1.4	0.56	2.5	0.055	2.0	454.4	6.1
11.1	521	163	0.32	32.9	0.23	0.073	1.3	0.58	2.2	0.057	1.7	456.0	5.9
12.1	395	249	0.65	25.0	0.07	0.074	1.4	0.58	2.1	0.057	1.6	458.2	6.0
13.1	442	86	0.20	28.3	0.07	0.075	1.3	0.59	1.9	0.058	1.4	463.5	5.9
14.1	223	84	0.39	14.1	0.14	0.073	1.4	0.59	3.2	0.058	2.9	455.0	6.2
15.1	379	401	1.09	24.3	0.33	0.074	1.3	0.56	2.7	0.054	2.4	461.8	6.0
16.1	116	94	0.84	8.3	0.72	0.083	1.5	0.61	4.9	0.054	4.7	511.9	7.6
16.2	175	77	0.45	10.8	0.32	0.071	1.5	0.58	4.1	0.059	3.9	444.9	6.2

Note: Pb_c and Pb^* indicate the common and radiogenic portions, respectively. Common Pb corrected using measured ^{204}Pb

0.77 and are consistent with a magmatic origin (Belousova et al., 2002). Radiogenic ^{206}Pb concentrations are higher, ranging from 13.7 to 112.3 ppm. The common ^{206}Pb concentrations are mostly very low (<1%), except for one datum (spot 12.1). The $^{206}Pb/^{238}U$ ages of 17 analytical spots range from 365 to 477.2 Ma, most of which are 442.1–477.2 Ma. An age of 426.3 Ma from a core (spot 12.2) is younger than the rim of the same grain (spot 12.1, 473.6 Ma); this core age may be unreliable owing to the presence of a small fracture and/or inclusions in the core. Spot 16.1 is highly discordant. In addition, considering other factors such as high common ^{206}Pb, the error and precision of ^{207}Pb and ^{206}Pb measurements, and the probable disturbance of zircons with bright rims, spots 6.1, 8.1, 9.1 and 12.1 were also regarded to be discordant points. Excluding discordant points, the remaining 11 concordant data range in age from 450.7 to 471.6 Ma and yield a weighted mean age of 462.5±3.6 Ma (MSWD=1.4).

The U and Th concentrations of zircons from the granitic stock range from 74 to 521 ppm and from 50 to 401 ppm, respectively, and Th/U ratios vary from 0.20 to 1.09. These grains are similar to those from the batholith in terms of their radiogenic ^{206}Pb and common ^{206}Pb concentrations. Seventeen analyses have $^{206}Pb/^{238}U$ ages between 444.8 and 511.9 Ma, with most (16) between 444.8 and 469.0 Ma. These 16 concordant data yield a weighted mean age of 457.8±3.1 Ma (MSWD=1.6). The oldest age of 511.9 Ma (spot 16.1) is from a zircon core. This age may represent the timing of captured zircons from the old basement.

In the Concordia diagrams of $^{206}Pb/^{238}U$ versus $^{207}Pb/^{238}U$ (Fig. 5), the 11 data points for zircon grains from the batholith plot as a group, as do the 16 data points for zircon grains from the stock. Consequently, the weighted mean $^{206}Pb/^{238}U$ ages of 462.5±3.6 Ma (MSWD=1.4) and 457.8±3.1 Ma (MSWD=1.6) are regarded as the best estimates of the crystallization age of the batholith and stock, respectively.

5.2 Major- and trace-element compositions

The whole-rock major- and trace-element compositions of seven samples from the batholith and two samples from the stock are listed in Table 2. The major-element concentrations have been recalculated on an anhydrous basis. In the SiO_2 vs. AR diagram (Fig. 6a, in which AR= $[Al_2O_3+CaO+(Na_2O+ K_2O)]$ /$[Al_2O_3+CaO-(Na_2O+K_2O)]$, all as wt% ratio), both granites plot in the "Alkaline" field, and, according to the SiO_2 vs. K_2O diagram (Fig. 6b), both fall in the "High-K Calc-Alkaline" field. The CIPW normative mineral modes demonstrate that the contents of quartz (Qz), albite (Ab), and orthoclase (Or) are dominant

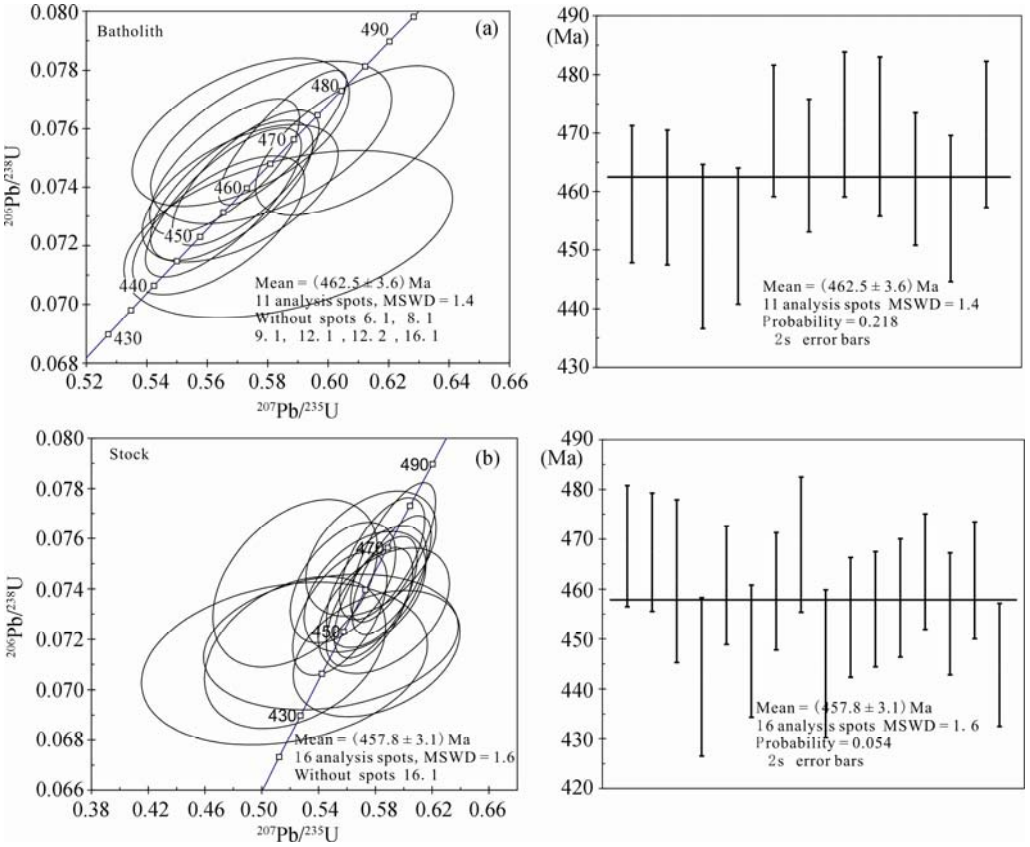

Fig. 5. SHRIMP zircon U–Pb concordia diagrams of the granitic batholith (a) and the granitic stock (b).

relative to anorthite (An). In general, the rocks are alkali feldspar granite according to the Q'-ANOR diagram (Fig. 6c, where Q'= Q/(Q+Or+Ab+An), and ANOR=100×An / (Or+An)), and are high in SiO_2 (75.18–78.60 wt%) and rich in alkalis ((Na_2O+K_2O) of 6.57–8.21 wt%, with AR of 2.90 to 3.65 and high K_2O contents of 3.51–4.84 wt%). The CaO, MgO, and total Fe_2O_3 contents range from 0.02 to 0.78 wt%, 0.17 to 0.69 wt%, and 0.56 to 1.94 wt%, respectively, with high $Mg^{\#}$(=100×atomic Mg/($Mg+Fe^{2+}$) =18.9–52.3) (Table 2). The granites are strongly peraluminous with A /CNK (=molar Al_2O_3/ ($CaO+Na_2O+K_2O$)) ratios of 1.09 to 1.39, A/NK (=molar Al_2O_3/(Na_2O+K_2O)) ratios of 1.15 to 1.45, and Al_2O_3 contents of 11.86 to 13.23 wt% (Table 2). All samples plot in the peraluminous field seen in Figure 6d, consistent with the high CIPW normative modes of corundum (1.13%–3.84%). The high Differentiation Index (DI (the total weight percentage of CIPW Qz, Or, Ab, Ne, Lc and Kp)=90.9–96.2) implies that the rocks are strongly differentiated.

The total REE (ΣREE) contents are relatively low (106.7–165.7 ppm) (Table 2). Chondrite-normalized REE patterns show that samples from the batholith are similar to those from the stock (Fig. 8a). All rocks show moderate fractionation of light REEs (LREEs) over heavy REEs (HREEs) {$(La/Yb)_N$=2.54–4.84}. The LREEs are moderately fractionated {$(La/Sm)_N$=2.06–2.81}, the HREEs are broadly flat {$(Gd/Yb)_N$=1.05–1.30}, and the rocks display pronounced negative Eu anomalies (δEu=0.20–0.35) (Table 2, Fig. 8a).

Both types of granite display obvious trace-element patterns with low Sr, Ba, and Zr contents and high Rb and Th contents (Table 2). Concentrations of Sr, Ba, and Zr range from 31.6 to 62.7 ppm, 209.1 to 301.3 ppm, and 87.2 to 144.0 ppm, respectively. Contents of Rb and Th are relatively high at 135.9 to 541.7 ppm and 12.7 to 17.4 ppm, respectively (Table 2). In a primitive-mantle-normalized spider diagram (Fig. 8b), the granitic batholith is compositionally similar to the granitic stock and exhibits clear negative anomalies in Ba, Sr, P, Ti, Nb, and Ta, and positive anomalies in Rb, Th, U, K, La, Nd, and Hf. The samples also have somewhat high 10,000×Ga/Al ratios of 2.1–2.7. The calculated zircon saturation temperatures (T_{Zr}) are 746 to 796°C (Table 3) based on the calibration of Watson and Harrison (1983).

5.3 Sr-Nd isotope compositions

The Sr–Nd isotopic data for the two granites are given in Table 4. Initial Sr–Nd isotopic compositions were calculated at t=462.5 Ma (for the batholith) and t=457.8 Ma (for the stock). The calculated initial $^{87}Sr/^{86}Sr$ ratios range from 0.513746 to 0.710025. The wide range of initial $^{87}Sr/^{86}Sr$ ratios and the unreasonably low ratios reflect the large range and high values of the $^{87}Rb/^{86}Sr$ ratios (8.62 to 72.88). High Rb/Sr samples with highly radiogenic Sr isotopic compositions can lead to large analytical uncertainties, especially for samples with very low Sr contents (<20 ppm) (Romer et al., 2012), and apparent values of less than ~0.7 probably have no petrogenetic significance (Jahn et al., 2000b). Therefore,

Table 2 Major oxides (wt%) and trace element (ppm) compositions of two granites in the Talate mining district

Samples	Batholith							Stock	
	T-01	T-02	T-03	T-04	T-05	T-06	T-07	T-69	T-70
SiO_2	78.60	76.75	77.63	77.35	77.73	78.59	77.42	76.41	75.18
TiO_2	0.07	0.07	0.06	0.06	0.07	0.06	0.14	0.20	0.18
Al_2O_3	12.31	12.81	12.49	12.13	11.86	12.25	12.38	12.47	13.23
TFe_2O_3	0.93	0.99	0.92	1.12	1.26	0.56	1.34	1.94	1.55
FeO	0.41	0.49	0.33	0.33	0.62	0.37	0.66	0.58	0.66
MnO	0.02	0.03	0.03	0.02	0.03	0.03	0.04	0.03	0.04
MgO	0.17	0.23	0.19	0.13	0.69	0.25	0.48	0.32	0.64
CaO	0.02	0.16	0.14	0.32	0.18	0.24	0.31	0.45	0.78
Na_2O	3.37	3.37	3.36	3.33	1.86	3.04	3.72	3.23	3.69
K_2O	3.65	4.84	4.78	4.63	4.71	4.34	3.51	3.89	3.80
P_2O_5	0.03	0.03	0.03	0.03	0.02	0.03	0.05	0.09	0.07
LOI	0.52	0.76	0.56	0.48	1.22	0.66	0.64	0.66	0.58
TOTAL	99.69	100.04	100.2	99.61	99.63	100.1	100	99.69	99.73
Na_2O+K_2O	7.02	8.21	8.14	7.96	6.57	7.38	7.23	7.12	7.49
Na_2O/K_2O	0.92	0.70	0.7	0.72	0.39	0.7	1.06	0.83	0.97
CaO/Na_2O	0.01	0.05	0.04	0.10	0.10	0.08	0.08	0.14	0.21
A/CNK	1.29	1.16	1.14	1.09	1.39	1.21	1.18	1.20	1.14
A/NK	1.30	1.19	1.17	1.15	1.45	1.26	1.25	1.31	1.30
AR	3.41	3.16	3.27	3.30	3.40	2.90	3.65	3.00	3.23
DI	95.5	95.7	96.2	95.6	92.3	95.2	93.7	92.4	90.9
Crn	2.84	1.82	1.61	1.13	3.48	2.2	2.02	2.37	1.81
Q	44.9	38.1	39.3	39.5	48.0	43.5	41.1	41.6	36.8
An	0.0	0.6	0.5	1.4	0.8	1.0	1.2	1.7	3.5
Ab	28.8	28.7	28.6	28.4	16.0	25.9	31.7	27.6	31.5
Or	21.8	28.8	28.4	27.6	28.3	25.8	20.9	23.3	22.7
A	50.5	56.9	56.4	54.7	43.9	50.7	50.8	49.1	50.0
P	0.0	1.2	1.0	2.8	1.2	2.0	3.0	3.5	7.7
$Mg^{\#}$	26.8	31.7	29.2	18.9	52.3	47.2	41.8	24.8	45.3
La	22.77	18.01	16.25	15.53	25.10	21.62	24.52	25.41	30.41
Ce	51.44	39.75	40.63	36.85	57.95	48.04	49.99	49.25	61.00
Pr	6.52	5.35	4.59	4.53	6.84	6.12	6.46	6.77	7.84
Nd	25.14	20.33	18.27	18.19	26.49	23.95	24.95	26.69	30.82
Sm	6.03	5.22	4.61	4.87	6.57	6.20	5.65	6.19	7.00
Eu	0.55	0.43	0.36	0.35	0.61	0.52	0.66	0.69	0.82
Gd	5.96	5.22	5.57	5.92	7.13	7.60	5.87	6.89	7.09
Tb	1.07	0.92	1.02	1.10	1.31	1.41	1.06	1.27	1.24
Dy	7.14	6.23	7.00	7.53	8.41	9.38	6.84	8.43	7.67
Ho	1.54	1.32	1.55	1.60	1.79	2.07	1.45	1.88	1.61
Er	4.40	3.87	4.52	4.51	4.96	5.89	4.14	5.19	4.32
Tm	0.67	0.60	0.70	0.69	0.76	0.88	0.64	0.81	0.67
Yb	4.43	3.96	4.52	4.38	4.92	5.74	4.29	5.41	4.51
Lu	0.65	0.59	0.67	0.66	0.73	0.84	0.64	0.77	0.66
∑REE	138.3	111.8	110.3	106.7	153.6	140.3	137.2	145.6	165.7
LREE	112.4	89.1	84.7	80.3	123.6	106.4	112.2	115.0	137.9
HREE	25.9	22.7	25.6	26.4	30.0	33.8	24.9	30.6	27.8
LR/HR	4.35	3.92	3.31	3.04	4.12	3.15	4.50	3.75	4.96
$(La/Sm)_N$	2.44	2.23	2.28	2.06	2.46	2.25	2.80	2.65	2.81
$(Gd/Yb)_N$	1.11	1.09	1.02	1.12	1.20	1.10	1.13	1.05	1.30
$(La/Yb)_N$	3.69	3.27	2.58	2.54	3.66	2.70	4.10	3.37	4.84
δEu	0.28	0.25	0.22	0.20	0.27	0.23	0.35	0.32	0.35
δCe	1.02	0.98	1.14	1.06	1.06	1.01	0.95	0.90	0.95
Sr	32.90	35.03	31.61	35.49	35.49	38.46	53.00	62.69	53.13
Rb	178.84	215.91	198.47	222.62	299.38	541.66	148.76	135.89	140.56
Ba	226.68	273.54	209.13	258.53	221.97	243.16	252.26	301.29	289.87
Th	14.32	16.01	12.68	13.22	14.89	16.02	15.94	16.60	17.43
U	2.95	3.18	2.96	4.09	3.98	2.12	2.69	2.60	3.38
Cr	0.57	0.72	0.36	0.99	0.42	0.95	2.01	4.09	3.56
Ta	1.23	1.44	1.30	1.84	1.65	7.50	1.33	1.35	1.26
Nb	12.22	13.16	13.92	13.44	15.62	19.00	12.01	13.86	12.68
Zr	87.23	87.34	90.84	87.19	92.43	93.91	120.83	143.98	136.44
Hf	3.43	3.54	3.64	3.56	3.66	3.81	4.67	5.09	5.09
Cu	1.21	2.91	2.36	3.65	4.85	1.23	2.98	9.39	6.24
Pb	14.26	18.09	15.61	19.92	17.52	19.04	14.84	17.88	20.63
Zn	15.99	24.51	18.66	17.53	28.02	20.95	26.00	20.35	22.43
Mo	0.09	0.10	0.05	0.21	0.07	0.05	0.13	0.19	0.34
V	0.34	0.61	0.16	0.29	2.32	0.36	5.22	12.23	10.31
Ni	0.22	4.25	0.08	3.56	0.61	0.46	1.19	2.44	3.59
Y	45.81	33.95	41.48	31.74	41.89	19.21	35.76	51.76	40.49
Co	1.20	0.71	0.59	0.82	1.61	0.79	2.08	3.07	2.31
Ga	14.04	14.92	15.00	15.41	15.99	17.85	14.54	16.13	15.74
Sc	5.94	6.89	7.24	6.77	7.54	6.53	7.05	9.14	7.81
Li	79.67	100.82	63.01	32.04	97.20	97.51	7.62	10.43	8.58

LOI is loss of ignition; AR=$[Al_2O_3+CaO+(Na_2O+K_2O)]/[Al_2O_3+CaO-(Na_2O+K_2O)]$ (wt% ratio); A/NK= $[Al_2O_3/(Na_2O+K_2O)]$ (molar ratio); A/CNK= $[Al_2O_3/(CaO+Na_2O+K_2O)]$ (molar ratio); $Mg^{\#}= 100\times Mg^{2+}/(Mg^{2+}+Fe^{2+})$ (molar ratio); δEu is a measure of the Eu anomaly when compare to Sm and Gd. $\delta Eu = 2\times Eu_N / (Sm_N + Gd_N)$. DI, Q (Quartz), An (Anorthite), Ab (Albite), Or (Orthosite), A (Alkaline feldspar), P (Plagioclase) and Crn (corundum) are from CIPW calculation.

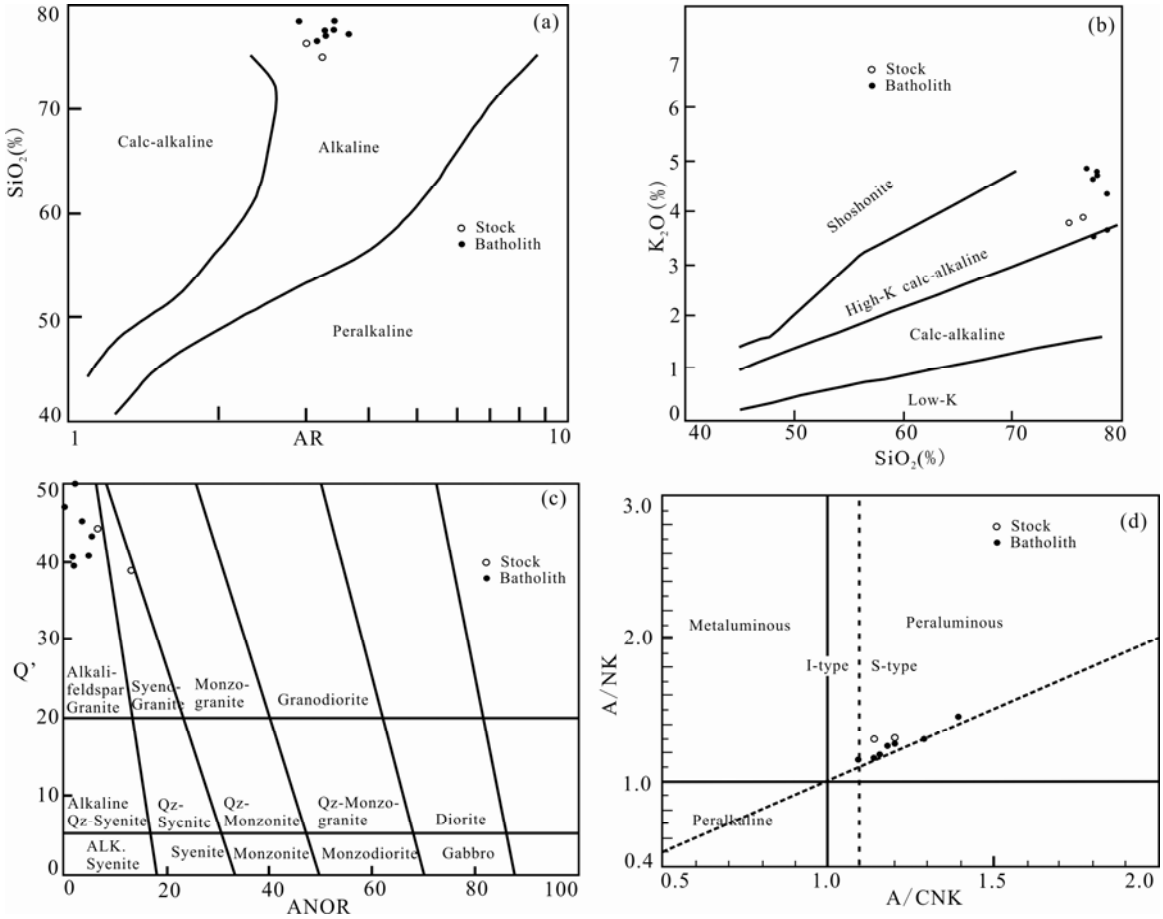

Fig. 6. AR vs. SiO_2 (after Wright, 1969) (a), SiO_2 vs. K_2O (after Le Maitre, 1989) (b), Q'-ANOR (after Streckeisen and Le Maitre, 1979) (c), A/NK - A/CNK (after Maniar and Piccoli, 1989) , and (d) diagrams of two granites studied here.
AR=$[Al_2O_3+CaO+(Na_2O+K_2O)]/[Al_2O_3+CaO-(Na_2O+K_2O)]$ (all as wt%); CIPW calculation: Q'=Q/(Q+Or+Ab+An), ANOR=100*An/(Or+An); A/NK= $[Al_2O_3/(Na_2O+K_2O)]$(molar ratio); A/CNK= $[Al_2O_3/(CaO+Na_2O+K_2O)]$ (molar ratio).

the samples analyzed in the present study do not yield meaningful initial Sr isotopic compositions because of their high Rb/Sr ratios (3.0–24.5) and low Sr contents (17.4–48.1 ppm) (Table 4). The Nd isotope data are more robust, and Sm/Nd ratios can provide a much less ambiguous constraint on the origin of granitic rocks (Jahn et al., 2000b). The two granitic bodies show a range of $\varepsilon_{Nd}(t)$ values of −1.21 to −0.08, with corresponding two-stage Nd model ages ranging from 1.20 to 1.30 Ga.

6 Discussion

6.1 Geochronology

The results of U–Pb dating are consistent with contemporaneous intrusion ages for the batholith and the stock, implying that they are different parts of the same magmatic suite that was emplaced during the middle Ordovician. However, according to the existing 1:200,000 geological map of the region, the batholith is considered to be a single pluton with a middle Hercynian age, supported by a zircon U–Pb age of 375±1 Ma (Wang et al., 2006)for the granite from the Daqiao area (Fig.1 b), some 15 km to the east of the batholith. In our opinion, these two clearly different ages represent two discrete phases of magmatic activity. The batholith should be divided into two different plutons at present, formed in Caledonian and middle Hercynian,respectively.

Table 3 The results of estimated saturated temperatures of zircons from two granites in the Talate mining district

Sample	T-1	T-2	T-3	T-4	T-5	T-6	T-7	T-69	T-70
M	1.04	1.19	1.20	1.25	0.95	1.11	1.16	1.14	1.24
Whole rock Zr (ppm)	87.2	87.3	90.8	87.2	92.4	93.9	120.8	144.0	136.4
lnDZr	8.65	8.64	8.61	8.65	8.59	8.57	8.32	8.14	8.20
T(°C)	761	761	753	746	772	762	780	796	784

TZr(°C)=12,900/(2.95+0.85×M+ $\ln D^{Zr}$, zircon/melt) (Watson and Harrison, 1983), where D^{Zr}, zircon/melt is the ratio of Zr concentrations (ppm) in zircon to that in the saturated melt (approximately equal to the Zr content in the whole rock), M=cation ratio (Na+K+2×Ca)/(Al × Si), representing the parameter for cation number ratio (total = 1), and T represents the absolute temperature.

The Talate Pb–Zn and Fe deposit is hosted within the late Silurian to early Devonian Kangbutiebao Formation. Consequently, the two Ordovician granites studied here are unrelated to the Talate deposit. In addition, there is no intrusive relationship between the granitic stock and the Kangbutiebao Formation because of the obvious earlier formation of the granite. This may be similar to a "tectonic window".

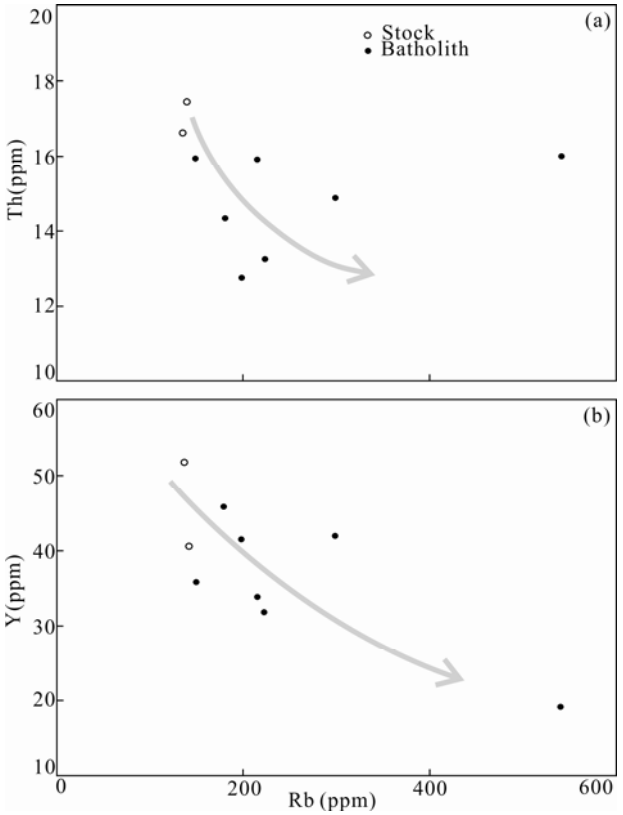

Fig. 7. Rb vs. Th (a) and Rb vs. Y (b) diagrams of two granites showing the trends of Th and Y contents that decrease with increasing Rb contents.

The oldest pluton yet identified in the Chinese Altay is the 479 Ma Jiadengyu granitoid (Cai et al., 2011a), a small granitic stock. There is no obvious magmatic gap from the early to middle Paleozoic (i.e., during the interval 460–375 Ma), and magmatism reached its climax during the Devonian (Cai et al., 2011a, b). However, the presence of significant volumes of 460 Ma granite as batholiths (Fig. 1b) suggests a magmatic activity peak during the early Paleozoic. Moreover, the study of Chai et al. (2010) and the present study document a long-lived phase of early Paleozoic peraluminous granitic magmatism in the Chinese Altay rather than a short pulse at 419–393 Ma (Cai et al., 2011b).

6.2 Petrogenesis

6.2.1 Classification

The major- and trace-element compositions of the samples from the batholith and stock are different from those of A-type granites but show a strong affinity with S-type granites. In Zr vs. 10000 × Ga/Al and FeO^T/MgO vs. SiO_2 diagrams (Fig. 9a, b), most samples fall into the fields of I- and S- rather than A-type granites. All samples plot in the field of S-type granite between muscovite and cordierite in the ACF diagram (Fig. 9c; White and Chappell, 1977). As mentioned in Section 5.2, the A/CNK values of the two granites range from 1.09 to 1.39, indicating that they are strongly peraluminous (Fig. 6d). Wu et al., (2007) and Chappell (1999) suggested that the trends of Th and Y with Rb are the effective ways to

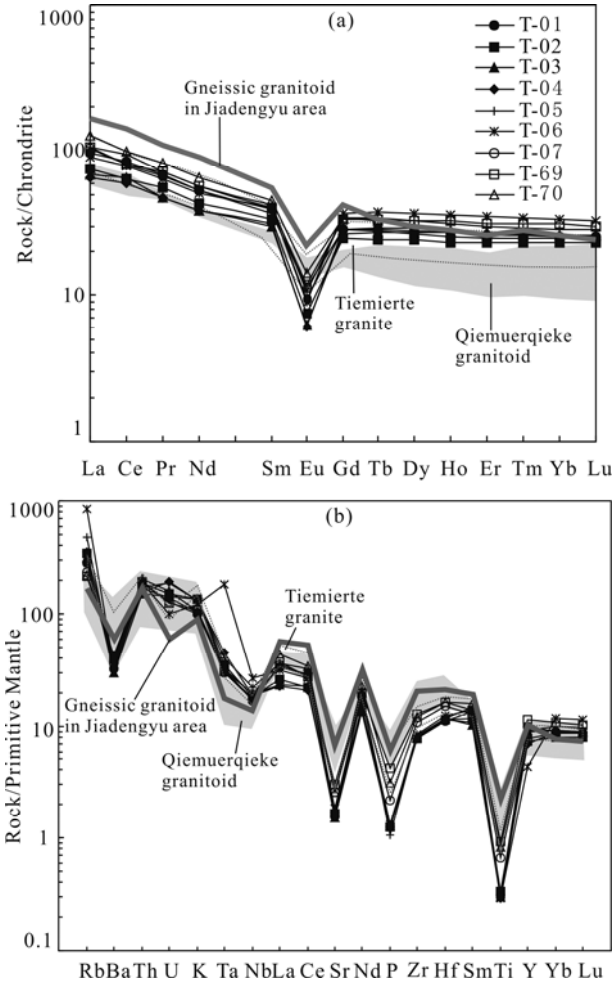

Fig. 8. Chondrite-normalized REE patterns (a) and Primitive mantle-normalized trace element spidergrams (b) for the two granitic plutons in the Talate mining district.
The gray area represents the compositional field of the Qiemuerqieke granitoids from Wang et al., (2006); the red dashed area represents the compositional field of the Tiemierte granite from Chai et al., (2010); the thick blue polyline represents the gneissic granitoid (453 Ma) from Sun et al., (2008) (Chondrite and primitive mantle content from Sun and McDonough, 1989).

distinguish S-type from I-type granites under high evolved case. Two granites studied here, with the negative correlation of Rb and Th, Rb and Y(Fig. 7a, b), further indicatethe affinity with S-type granites(Chappell, 1999). In addition, the two granites contain peraluminous minerals, such as muscoviteand cordierite, and all samples show high normative corundum content, ranging from 1.13% to 3.48% (Table 2). In addition, xenocrystic zircons (e.g., grains with an age of 511.9 Ma, Table 1) are present within the plutons, similar to most S-type granites (e.g., Keay et al., 1999; Cai et al., 2011b; Dan et al., 2014a, b). In summary, all the evidence indicates that the two Ordovician plutons are S-type granites, similar to the Ordovician Tiemierte batholith (Chai et al., 2010), but distinct from coeval I-type gneissose granitic stocks from the Jiadengyu area (Sun et al., 2008, 2009, Cai et al., 2011a) and the Qiemuqiek batholith further to the south (Wang et al., 2006). Thus, two genetic types of granite are

Table 4 The Nd and Sr isotopic compositions of two granites in the Talate mining district

Sample	Batholith							Stock	
	T-01	T-02	T-03	T-04	T-05	T-06	T-07	T-69	T-70
Rb(ppm)	200.7	226.4	222.9	228.5	318.3	569.2	166.2	142.6	154.1
Sr(ppm)	18.4	20.0	17.4	20.3	19.8	23.2	39.4	48.1	39.4
$^{87}Rb/^{86}Sr$	32.22	33.34	37.97	33.31	47.52	72.88	12.31	8.62	11.39
$^{87}Sr/^{86}Sr$	0.891988	0.901508	0.922625	0.910576	0.903161	0.993986	0.791104	0.760220	0.772721
±2σ	0.000011	0.000014	0.00001	0.00001	0.000013	0.000012	0.000011	0.000011	0.000011
$(^{87}Sr/^{86}Sr)_i$	0.679676	0.681853	0.672423	0.691115	0.59006	0.513746	0.710025	0.704007	0.698414
Sm(ppm)	6.8	6.0	11.2	4.9	6.6	11.3	5.6	6.6	7.0
Nd(ppm)	29.4	24.9	43.5	18.2	24.8	46.3	23.3	27.2	29.6
$^{147}Sm/^{144}Nd$	0.14006	0.14607	0.15606	0.16380	0.16191	0.14700	0.14441	0.14592	0.14329
$^{143}Nd/^{14}4Nd$	0.512450	0.512473	0.512472	0.512523	0.512487	0.512484	0.512417	0.512425	0.512443
±2σ	0.000011	0.000015	0.000012	0.000013	0.000010	0.000009	0.000011	0.00001	0.000010
$(^{143}Nd/^{144}Nd)_i$	0.512025	0.512031	0.511999	0.512027	0.511996	0.512038	0.511980	0.511987	0.512014
$\varepsilon_{Nd}(t)$	−0.34	−0.22	−0.84	−0.30	v0.90	v0.08	−1.21	−1.20	−0.67
T_{2DM}(Ga)	1.22	1.21	1.26	1.22	1.27	1.20	1.30	1.29	1.25
$f_{Sm/Nd}$	−0.29	−0.26	−0.21	−0.17	−0.18	−0.25	−0.27	−0.26	−0.27

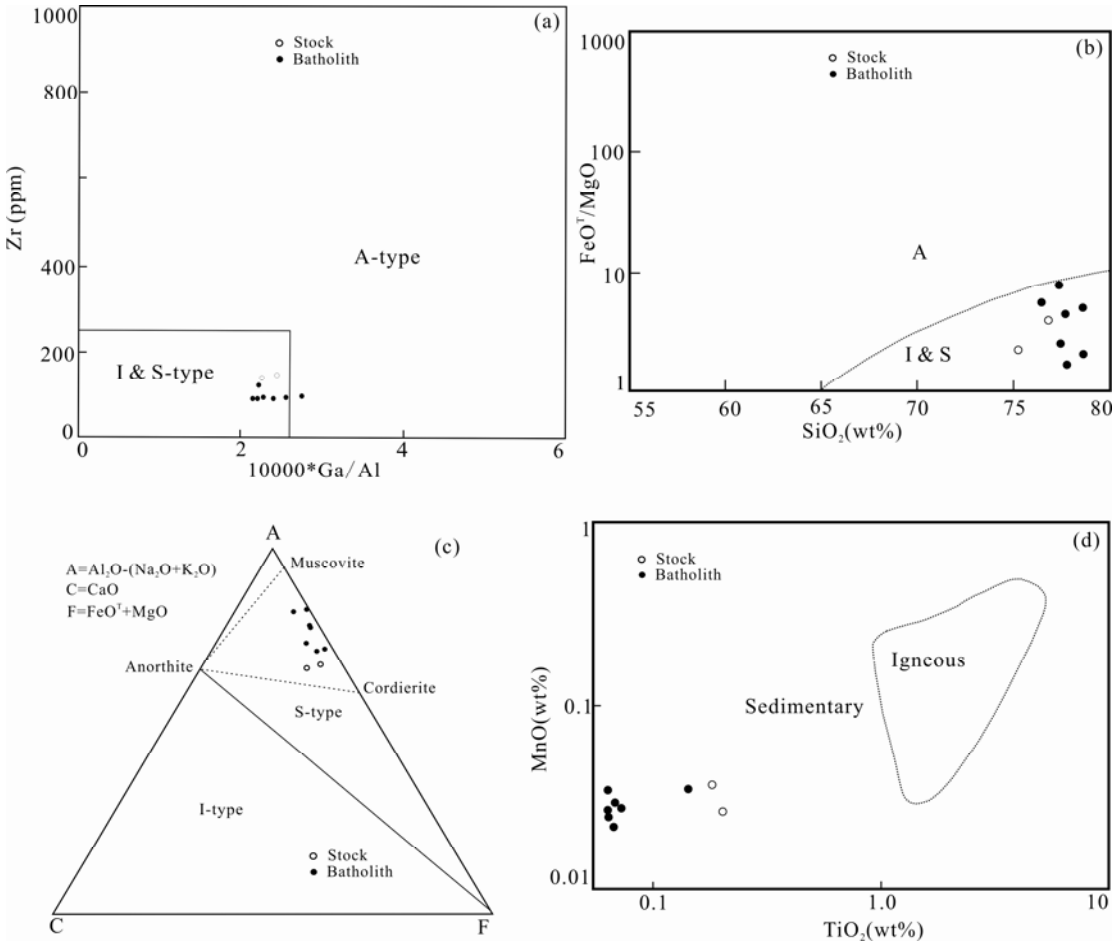

Fig. 9. Plots of Zr vs. 10000´Ga/Al (a) (from Whalen et al., 1987), FeO^T/MgO vs. SiO_2 (b) (from Eby, 1990), A-C-F (c) (from White and Chappell, 1977) and MnO vs. TiO_2 (d) (from Misra, 1971) for the peraluminous granites in the north of the Talate mining district.

present in the early Paleozoic Chinese Altay, as they are in the late Paleozoic Chinese Altay.

6.2.2 Magmatic source

The source of S-type granites is generally considered to be the partial melting of metasedimentary rocks (metapelite or metagreywacke) under water-undersaturated conditions (Patiño Douce and Harris, 1998; Sylvester, 1998; Visonà and Lombardo, 2002; Visonà et al., 2012). However, different models for the petrogenesis of S-type granite have also been suggested. Ellis and Thompson (1986) considered an origin involving the partial melting of basaltic rocks and/or amphibolites under water-saturated conditions. Patiño Douce (1997, 1999)

proposed that S-type granites could be produced via the partial melting of biotite-bearing tonalite and granodiorite at pressures of 8 kbar and above, with clinopyroxene in the residue. Moreover, Miller (1985) considered that the majority of peraluminous rocks are derived largely from intermediate to felsic crustal sources, including both immature sedimentary rocks and metaigneous rocks, or even metaluminous mafic sources. In recent years, a hybrid origin combining mantle-derived and intracrustal components with supracrustal components (metasediments) has been proposed for S-type granites in orogenic belts such as the Chinese Altay (Cai et al., 2011b), the Lachlan Fold Belt in SE Australia (Clemens, 2003; Healy et al., 2004), and the Himalayan belt (Zhu et al., 2009).

On the TiO_2 vs. MnO diagram of Mirsa (1971), all samples plot in the field of sediments and away from the igneous field (Fig. 9d), indicative of a metasedimentary origin. The high A/CNK values (1.09–1.39) and high normative corundum contents (1.13%–3.48%) from the two Ordovician S-type granites studied here also strongly support a metasedimentary source. The high Rb/Sr (2.2–14.1) and Rb/Ba (0.45–2.23) ratios of these granites may indicate that the source magma was derived mainly from formerly clay-rich rocks (i.e., metapelite; Fig. 10a). This is consistent with the Al_2O_3 / (MgO + FeO^T) vs. CaO / (MgO + FeO^T) diagram, in which all samples plot in the field of partial melts from metapelitic sources, with two samples in the transition between metapelite and metagraywacke (Fig. 10b). The low CaO/Na_2O ratios (mostly <0.1) of all samples are also consistent with a metapelite rather than a metagraywacke source (Sylvester, 1998). Two samples from the stock plot in the overlap between metagraywacke and metapelite (Fig. 10b), implying a small component of metagraywacke in the source. Moreover, experimental results have indicated that strongly peraluminous granites are derived largely from the partial melting of Al-rich crust (Green, 1995) and that the melts have different features reflecting the different compositions of the crustal sources (Altherr and Siebel, 2002).

The high K and Rb and relatively low Na and Ca contents of the granites studied here suggest that they might have resulted from the dehydration-melting of mica-bearing sources rather than of amphibole-bearing sources (Zhao et al., 2007). The distinctive depletion in Ba and the old two-stage model ages (1.20–1.30 Ga) are consistent with a highly mature crustal source (Ma et al., 2004). Peraluminous melts have high Rb/Sr (>3) and low Sr/Ba (<0.2) ratios under water-undersaturated conditions, but low Rb/Sr (<1.6) and high Sr/Ba (>0.5) ratios under water-saturated conditions (Li et al., 2005 and references therein). The Rb/Sr (mostly >3) and Sr/Ba (0.13-–0.21, mostly <0.20) ratios of the Ordovician granites in the Talate mining district indicate water-undersaturated partial melting. The two Ordovician granites have a mainly crustal geochemical signature, with low Nb/Ta (2.5 to 10.7) and Zr/Hf (24.5 to 28.3) ratios relative to primitive mantle (17.8 and 37, respectively; McDonough and Sun, 1995) but close to average continental crust (11 and 33, respectively; Taylor and McLennan, 1985). Li et al. (2006) proposed that a microcontinent occurred in the Chinese Altay as a metamorphic basement mainly consists of Proterozoic materials. The Mesoproterozoic Nd model ages (1.2 to 1.3 Ga) of the two Ordovician granites and its $\varepsilon_{Nd}(t)$ values (−1.21 to −0.08) close to the value of the metamorphic basement (about −5, Chen and Jahn, 2002; Wang et al., 2009) both suggest that the parental magmas of these granites might have been mainly derived from the Mesoproterozoic sources of this basement, but with some input from mantle-derived (juvenile) components.

Zircon is an early-crystallizing accessory mineral in granitic magmas that is very sensitive to temperature (Miller et al., 2003). Thus the zircon saturation temperature can approximate the near-liquidus temperature of granitic rocks (King et al., 1997). The zircon temperature can be calculated by the following equation (Watson and Harrison, 1983): $\ln D^{Zr(Zircon/melt)}$ +3.80+0.85(M−1) = 12900/T. For the Ordovician granites studied here, the calculated zircon saturation temperatures range from 746 to 796 °C (Table 3), indicative of medium to high temperature.

The high Yb (3.96–5.74 ppm) and Y (19.21–51.76 ppm) contents and high Zr/Sm (14.0–23.3) ratios for the two granites suggest that the partial melting of the source took place away from the stable field of garnet (Defant et al., 2002). The REE patterns, especially the slight depletion in HREEs ($(La/Yb)_N$= 2.54 to 4.84), also indicate that there was little garnet in the residue. In addition, the strong

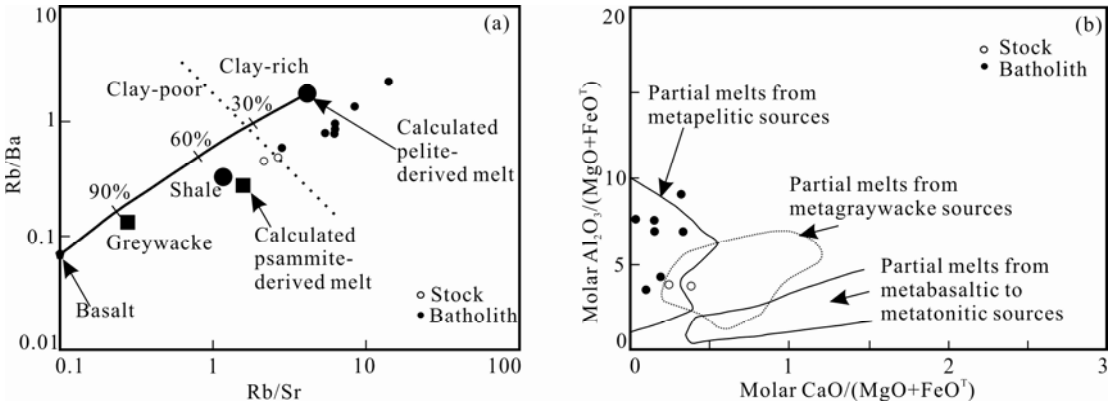

Fig. 10. Plots of (a) Rb/Sr vs. Rb/Ba (after Patiño and Harris,1998, and Sylvester, 1998), and (b) Molar Al_2O_3/(MgO FeO^T) vs. molar CaO/(MgO FeO^T) (After Altherr et al.,2000 and Gerdes et al.,2002) of the peraluminous granites in the north of the Talate mining district.

negative anomalies for Eu, Sr, P, and Ti are consistent with source rock residues containing substantial amounts of plagioclase, apatite, and ilmenite, implying low pressures of melting. Thus, the compositions of the peraluminous granites are comparable with those of melts produced by the dehydration-melting of metapelite at low pressure (Fig. 11a), suggesting that their precursor magmas were derived from shallow crustal levels. This is consistent with the Qz–Ab–Or phase diagram that implies pressures of ≤1 kbar (Fig. 11b).

In summary, these Ordovician granites were probably producedby partial melting under water-undersaturated, medium- to high-temperature and low-pressure conditions and derived mainly from Mesoproterozoicmica-rich metapelitic source rockswith minor contamination from a mantle component.

6.3 Tectonic setting

Previous studies have indicated the existence of a microcontinent or fragments of Proterozoic basement in the Chinese Altay (Li et al., 2006; Li and Poliyangsiji, 2001; Wang et al., 2006). Increasingly, the evidence shows that early to middle Paleozoic magmatism in the Chinese Altay was generated in an active margin setting (Lou, 1997; Windley et al., 2002; Shan et al., 2005; Sun et al., 2008; Wang et al., 2006; Chai et al., 2010; Cai et al., 2011a; Wang et al., 2011). For the Ordovician granitoids in the Chinese Altay, the Qiemuqiek batholith to the south (462 Ma, Wang et al., 2006) and the Tiemierte batholith to the north (459 Ma, Chai et al., 2010) have been thought to have formed in a continental arc setting related to subduction, similar to the Yinisala granodiorite (452.0 Ma, Wang et al., 2017) in the north of the West Junggar. Two stocks of gneissic granitoid (453 Ma, Sun et al., 2008; 479 Ma, Cai et al., 2011a) in the west of the Chinese Altay have been suggested to have formed also in a subduction-related environment. The Ordovician granitic plutons studied here show REE and trace-element similarities to other Ordovician plutons (Fig. 8), implying a common environment of formation. Their different genetic types, namely I-type for the Qiemuqiek batholith and gneissic granitoids and S-type for the Tiemierte batholith and the plutons studied herein, likely reflect differences only in the magmatic source rocks.

The negative anomalies in P, Nb, and Ti exhibited by the studied granites are shared by arc-related granites (e.g., Sajona et al., 1996). Various tectonic discrimination diagrams (e.g., Nb vs. Y and Rb vs. (Yb+Ta), not shown here) also indicate that these granites plot in the "VAG" (volcanic arc granite) field. Furthermore, the negative anomalies in Ba, P, Nb, Ta, Ti, and, in particular, Sr, as well as the pronounced positive anomalies in Rb, Th, K, and La, can also be explained by the involvement of crustal melts related to subduction (Wang et al., 2006). The negative $\varepsilon_{Nd}(t)$ values (−1.21 to −0.08) and the Mesoproterozoic whole-rock two-stage Nd model ages (1.20–1.30 Ga) also suggest that ancient crustal materials contributed to the granitoids. It is therefore concluded that the overall geochemical and isotopic features support a continental arc setting and the existence of an early Paleozoic subduction regime in the Chinese Altay.

It is commonly considered that peraluminous granitoids of crustal origin are generally formed in collisional orogens and are emplaced near the climax of collisional orogenesis or in a post-collisional setting (Altherr et al., 1995; Pamic et al., 1996; Finger et al., 1997; Searle et al., 1997; Sylvester, 1998; Barbarin, 1996, 1999). However, in the Chinese Altay, previous research by Cai et al. (2011b) and Chai et al. (2010), with which our results concur, suggested that the peraluminous or strongly peraluminous granitoids formed during subduction of the Paleoasian Ocean during the early Paleozoic, and might record the products of shallow melting during the early stages of subduction.

A remaining problem is establishing the source of heat required for the partial melting of the source rocks, as subduction of oceanic lithosphere is unlikely to provide sufficient heat for the partial melting of supracrustal rocks at shallow depths. It is therefore considered that mantle-derived magmas might have provided sufficient additional

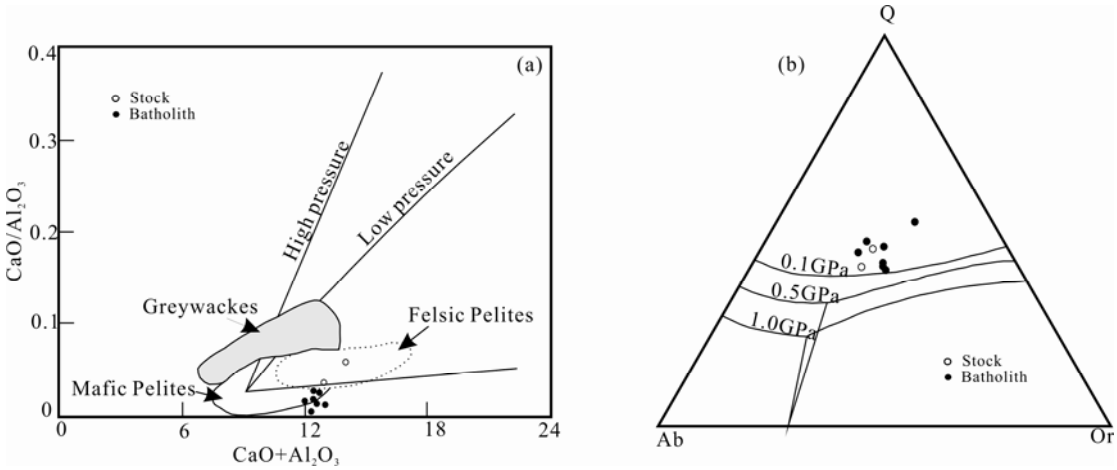

Fig. 11 (a) Compositions of the studied Ordovician peraluminous granites, compared with experimental melts from the dehydration-melting of various kinds of metasediment (after Patiño Douce, 1999). (b) CIPW-normative Qt-Ab-Or diagramwith low-pressure melt compositions at 0.1, 0.5 and 1.0 GaPa (after Johannes and Holtz, 1996).
The thick solid lines in Fig. 11a are reaction curves based on hybridization of high-Al olivine tholeiite with metapelite at low pressure (≤5 kbar) and high pressure (12–15 kbar).

heat for partial melting, and it is likely that the generation of partial melting occurred under a specific geothermal condition in a subduction setting. Previous studies have indicated the existence of a high geothermal gradient, high heat flow, and a mantle with anomalously low seismic velocity (<8 km/s) beneath the southern margin of the Chinese Altay during the early Paleozoic (Zeng et al., 2007), and these features may have played a crucial role in the formation of the early Paleozoic granites.

A ridge subduction model, which was first suggested by Windley et al. (2007), accounts for the evolutionary history of the Chinese Altai during the Devonian (Cai et al., 2011b). Similarly, here it is proposed that Ordovician ridge subduction with the associated opening of a slab window controlled the tectonic evolution of the region during the early stages of subduction. It is also suggested that the thermal, physical, and chemical anomalies in rocks of the Chinese Altay reflect such an Ordovician ridge subduction and the opening of a slab window at relatively shallow levels that triggered upwelling and the partial melting of asthenospheric mantle.Substantial volumes of mantle-derived magma underplated and/or were emplaced into the middle to upper crust and triggered extensive partial melting of the crust at shallow levels to generate diverse igneous rocks, including peraluminous S-type granites from the partial melting of metapelitic rocks (e.g., Tiemierte granite and granites studied herein) and metaluminous I-type granites from the partial melting of intermediate–mafic igneous rocks (e.g., the Qiemuerqieke granite). This tectonic scenario in the Chinese Altay during the early Paleozoic can be supported by: (1) the emplacement ages of S-type granites (e.g., Chai et al., 2010 and this paper) overlap those of the metaluminous I-type granites (e.g., Wang et al., 2006; Sun et al., 2008; Cai et al., 2011a) and they all share the features with high-T and low-P. These kinds of geological features commonly occur in modernWestern North and Central America, south Chile, where ridge subduction was considered as a chief mechanism responsible for the magmatic activity (Sisson et al., 2003); (2) in the South Altay, the late Ordovician–early Silurian Mayinebo ophiolite (437±12 Ma, Zhang et al., 2012) and the late Ordovician Tangbale ophiolite (447 Ma, Zhang and Huang, 1992) contain diverse genetic types of basalt. The former basalt shares MORB features (Zhang et al., 2012), distinct from the latter arc-back basalt (Zhang and Huang, 1992). The ridge-subduction tectonic setting is useful to form these rocks with complicated sources (Sun et al., 2009).

7 Conclusions

Based on SHRIMP zircon U–Pb dating, whole-rock geochemistry, and Sr–Nd isotopic data from two strongly peraluminous granites in the north of the Talate mining district in the Chinese Altay, the following conclusions can be drawn:

(1) Both granites were emplaced during the early Paleozoic, coeval with a magmatic peak at ~460 Ma in the Chinese Altay. There is evidence for long-lived early Paleozoic peraluminous granitic magmatism in the Chinese Altay, rather than a short-lived pulse of magmatism at 419–393 Ma (Cai et al., 2011b).

(2) The two studied granites are strongly peraluminous S-type granites. Their precursor magmas were derived from relatively shallow crustal levels ($P \leq 1$ kbar) at temperatures of around 750–800 °C. The two bodies have no genetic relationship with the formation of the younger Talate deposit.

(3) The Ordovician peraluminous granites were derived mainly from the dehydration-melting of mica-rich Mesoproterozoic metapelitic source rockswith a contribution from mantle-derived components.

(4) The early Paleozoic peraluminous and coeval I-type granites in the Chinese Altay were likely emplaced during the early stages of subduction of an active continental arc. A ridge subduction model is proposed as the geodynamic setting, in which substantial mantle-derived magmas were generated by ridge subduction and the opening of a slab window at relatively shallow levels. Mantle-derived magmas underplated, or were emplaced into, the middle to upper crust, triggering extensive partial melting of shallow crustal rocks to generate diverse igneous rocks.

Acknowledgments

This study was financially supported the National Key S&T Support Program of China (2006BAB07B02-01, 02), the Fundamental Research Funds for Scientific Institution (JYYWF20180104) and Geological investigation (DD20190398). Gratitude is extended to Suohan Tang (Institute of Geology) and the staff (National Research Center) from the Chinese Academy of Geological Sciences for their help with isotopic and geochemical analyses. Special thanks are extended to engineer Xu from the Talate Resource Co. Ltd. for his generous field support. Constructive reviews and suggestions by the editors and anonymous reviewers led to significant improvements in the manuscript.

Manuscript received Sept. 12, 2018
accepted Jan. 28, 2019
associate EIC HAO Ziguo
edited by Susan Turner and FEI Hongcai

References

Altherr, R., Lugović, B., Meyer, H.P., and Majer, V., 1995. Early Miocene post-collisional calcalkaline magmatism along the easternmost segment of the Periadriatic fault system (Sloveniand Croatia). Mineralogy and Petrology, 54: 225–247.

Altherr, R., Holl, A., Hegener, E., Langer, C. and Kreuzer, H., 2000. High potassium, calc-alkaline plutonism in the European variscides: northern Vosges (France) and northern Schwarzwald (Germany). Lithos, 50: 51–73.

Altherr, R., and Siebel, W., 2002. I-type plutonism in a continental back-arc setting: Miocene granitoids and monzonites from the central Aegean Sea, Greece. Contributions to Mineralogy and Petrology,143: 397–415.

Badarch, G., Cunningham, W.D., and Windley, B.F., 2002. A new terrane subdivision for Mongolia: implications for the Phanerozoic crustal growth of Central Asia. Journal of Asian Earth Sciences, 21: 87–110.

Barbarin, B., 1996. Genesis of the two main types of peraluminous granitoids. Geology, 24: 295–298.

Barbarin, B., 1999. A review of the relationships between

granitoid types, their origins and their geodynamic environments. Lithos, 46: 605–626.
Belousova, E.A., Griffin, W.L. and Oreilly, S.Y., 2002. Igneous zircon: Trace element composition as an indicator of source rock type. Contributions to Mineralogy and Petrology, 143: 602–622.
Buslov, M.M., Watanabe, T., Safonova, I.Y., Iwata, K., Travin, A., and Akiyama, M., 2002. A Vendian-Cambrian island arc system of the Siberian continent in Gorny Altai (Russia, Central Asia). Gondwana Research, 5: 781–800.
Buslov, M.M., Fujiwara, Y., Iwata, K., and Semakov, N.N., 2004. Late Paleozoic-Early Mesozoic geodynamics of Central Asia. Gondwana Research,7: 791–808.
Cai, K.D., Sun, M., Yuan, C., Zhao, G.C., Xiao, W.J., Long, X.P., and Wu, F.Y., 2011a. Prolonged magmatism, juvenile nature and tectonic evolution of the Chinese Altai, NW China: Evidence from zircon U-Pb and Hf isotopic study of Paleozoic granitoids. Journal of Asian Earth Sciences, 42: 949–968.
Cai, K.D., Sun, M., Yuan, C., Zhao, G.C., Xiao, W.J., Long, X.P., and Wu, F.Y., 2011b.Geochronology, petrogenesis and tectonic significance of peraluminous granites from the Chinese Altai, NW China. Lithos, 127: 261–281
Chai, F.M., Mao, J.W., Dong, L.H., Yang, F.Q., Liu, F., Geng, X.X., and Zhang, Z.X., 2009. Geochronology of metarhyolites from the Kangbutiebao Formation in the Kelang basin, Altay Mountains, Xinjiang: Implications for the tectonic evolution and metallogeny. Gondwana Research, 16: 189–200.
Chai, F.M., Dong, L.H., Yang, F.Q., Liu, F., Geng, X.X., and Huang, C.K., 2010. Age, chemistry and petrogenesis of Tiemierte granites in the Kelang basin at the southern margin of Altay, Xinjiang. Acta Petrologica Sinica, 26(02): 377–386 (in Chinese with English abstract).
Chappell, B.W., 1999. Aluminium saturation in I and S-typegranites and the characterization of fractionatedhaplogranites. Lithos, 46: 535-551.
Chen, B., and Jahn, B.M., 2002. Geochemical and isotopic studies of the sedimentary and granitic rocks of the Altai Orogen of Northwest China and their tectonic implications. Geology Magazine,139: 1–13.
Clemens, J.D., 2003. S-type granitic magmas-petrogenetic issues, models and evidence. Earth Science Review, 61: 1–18.
Coleman, R.G., 1989. Continental growth of Northwest China. Tectonics, 8: 621–635.
Dan, W., Li, X.H., Wang, Q., Wang, XC., and Liu, Y., 2014a. Neoproterozoic S-type granites in the Alxa Block, westernmost North China and tectonic implications: In situ zircon U-Pb-Hf-O isotopic and geochemical constraints. American Journal of Science, 314: 110–153.
Dan, W., Li, X.H., Wang, Q., Wang, XC., Liu, Y., and Wyman, D.A., 2014b. Paleoproterozoic S-type granites in the Helanshan Complex, Khondalite Belt, North China Craton: Implications for rapid sediment recycling during slab break-off. Precambrian Research, 254: 59–72.
Defant, M.J., Xu, J.F., and Kepmhinskas, P., 2002. Adakites: some variations on a theme. Acta Petrologica Sinica, 18: 129–142.
Du, L.L., Zhuang, Y.X., Yang, C.H., Wan, Y.S., and Wang, X.H., 2005. SHRIMP U-Pb zircon chronology of fine-grained amphibolite in the Mengjiatun area, western Shandong. Acta Geoscientic Sinica, 26(05): 429–434 (in Chinese with English abstract).
Eby, G.N., 1990. The A-Type granitoids: a review of their occurrence and chemical characteristics and speculations on their petrogenesis. Lithos, 26: 115–134.
Ellis, D.J. and Thompson, A.B., 1986. Subsolidus and partial melting reactions in the quartz excess CaO + MgO + Al_2O_3 + SiO_2 + H_2O system under water-excess and water deficient condiments to 10 kb: some implications for the origin of peraluminous melts from mafic rocks. Journal of Petrology, 27: 91–121.
Finger, F., Roberts, M.P., Haunschmid, B., Schermaier, A., and Steyrer, H.P., 1997. Variscan granitoids of central Europe: their typology, potential sources and tectonothermal relations. Mineralogical Petrology, 61: 67–96.
Green, T.H., 1995. Significance of Nb/Ta as an indicator of geochemical process in the crust-mantle system. Chemical Geology, 120: 347–359.
Gerdes, A., Montero, P., Bea, F., Fershater, G., 2002. Peraluminous granites frequently with mantle-like isotope compositions: the continental-type Murzinka and Dzhabyk batholiths of the eastern Urals. International Journal of Earth Sciences, 91: 3–19.
He, G.Q., Cheng, S.D., Xu, X., Li, J.Y., and Hao, J., 2004. An Introduction to the Explanatory Text of the Map of Tectonics of Xinjiang and Its Neighbouring Areas. Beijing: Geological Publishing House, 65pp. (in Chinese with English abstract).
Healy, B., Collins, W.J., and Richards, S.W., 2004. A hybrid origin for Lachlan S-type granites: the Murrumbidgee Batholith example. Lithos, 78: 197–216.
Hong, D.W, Wang, S.G., Xie, X.L., Zhang, J.S, and Wang, T., 2003. Metallogenic province derived from mantle sources: Nd, Sr, S and Pb isotope evidence from the Central Asian orogenic belt. Gondwana Research, 6: 711–728.
Hu, A.Q., Jahn, B.M., Zhang, G.X., Chen, Y.B., and Zhang, Q.F., 2000. Crustal evolution and Phanerozoic crustal growth in northern Xinjiang: Nd isotopic evidence, Part I. Isotopic characteristics of basement rocks. Tectonophysics,328: 15–51.
Jahn, B.M., Wu, F.Y. and Chen, B., 2000a. Masssive granitoid generation in Central Asia: Nd isotopic evidence and implication for continental growth in the Phanerozoic. Episodes,23: 82–92.
Jahn, B. M., Wu, F.Y., and Chen, B., 2000b. Granitoids of the Central Asian Orogenic Belt and continental growth in the Phanerozoic. Transactions of Royal Society Edinburgh Earth Science,91: 181–193.
Johannes, W., and Holtz, F., 1996. Petrogenesis and Experimental Petrology of Granitic Rocks. Berlin: Springer, 1 –335.
Keay, S., Steele, D., and Compston, W., 1999. Identifying granite sources by SHRIMP U-Pb zircon geochronology: an application to the Lachlan foldbelt. Contribution Mineralogy and Petrology,137: 323–341.
King, P.L., White, A.J.R., Chappell, B.W., and Allen C.M., 1997. Characterization and origin of aluminous A-type granites from the Lachlan Fold Belt, southeastern Australia. Journal of Petrology, 38: 371–391.
Le, M.R.W., 1989.A Classification of Igneous Rocks and Glossary Terms. Oxford: Recommendations of the International Union of Geological Sciences Subcommission on the Systematics of Igneous Rocks Blackwell Scientific Publications, 1–193.
Li, P.C., Xu, D.R., Chen, G.H., Xia, B., He, C.L., and Fu, G.G., 2005. Constraints of petrography, geochemistry and Sr-Nd isotopes on the Jinjing granitoids from northeastern Hunan Province, China: Implications for petrogenesis and geodynamic setting. Acta Petrologica Sinica, 21(03): 921–934 (in Chinese with English abstract).
Li, H.J., He, G.Q., Wu, T.R., and Wu, B., 2006. Confirmation of Altai-Mongolia microcontinent and its implications. Acta Petrologica Sinica, 22(05), 1369–1379 (in Chinese with English abstract).
Li, J.Y., Xiao, W.J., Wang, K.Z., Sun, G.H., and Gao, L.M., 2003. Neoproterozoic-Paleozoic tectonostratigraphy, magmatic activities and tectonic evolution of eastern Xinjiang, NW China. In: Mao, J.W., Goldfarb, R.J., Seltman, R., Wang, D.H., Xiao, W.J., and Hart, C. (Eds.), Tectonic Evolution and Metallogeny of the Chinese Altay and Tianshan. London: CERCAMS/NHM, IAGOD Guidebook Series, 10: 31–74.
Li, T.D., and Poliyangsiji, B.H., 2001. Tectonics and crustal evolution of Altay in China and Kazakhstan.Xinjiang Geology, 19(01): 27–32 (in Chinese with English abstract).
Liu, F., Li, Y.H., Mao, J.W., Yang, F.Q., Chai, F.M., Geng, X.X., and Yang, Z.X., 2008. The SHRIMPU-Pb ages of Abagong granites in the Altaid Orogen and its geologic implication. Acta Geoscientica Sinica, 29(6): 795–804 (in Chinese with English abstract).
Liu, F., Zhang, Z.X., Li, Q., Zhang, C., and Li, C., 2014. New precise timing Constraint for the Keketuohai No. 3 pegmatite in Xinjiang, China, and identification of its parental pluton: Ore Geology Reviews, 56: 209–219.

Liu, G.R., Dong, L.H., Gao, F.P., Chen, J.X., Zhao, H., Wang, D.S., Song, Z.Y., He, L.X., Qin, J.H., 2010. LA-ICP-MS U-Pb zircon dating and geochemistry of the devonian granites from the middle Kelan River Valley of Altay in Xinjiang.Acta Geoscientica Sinica, 31(04): 519–531 (in Chinese with English abstract).

Lou, F.S., 1997. Characteristics of Late Caledonian granites in the Nuerte area, Altay. Jiangxi Geology. 11(03): 60–66 (in Chinese with English abstract).

Ludwig, K.R., 2001.Users Manual for Isoplot/Ex rev. 2.49. Berkeley Geochronology Centre Special Publication,1–56.

Ma, C.Q., Ming, H.L. and Yang, K.G., 2004. An Ordovician magmatic arc at the northern foot of Dabie mountains: Evidence from geochronology and geochemistry of intrusive rocks. Acta Petrologica Sinica, 20(03): 393–402 (in Chinese with abstract).

Maniar, P.D., and Piccoli, P.M., 1989. Tectonic discrimination of granitoids. The Geological Society of America Bulletin, 101: 635-643.

McDonough, W.F. and Sun, S.S., 1995. The composition of the earth. Chemical Geology, 120: 223–253.

Mei Houjun, Yang Xuechang, Wang Junda, Yu Xueyuan, Liu Tiegeng, and Bai Zhenghua, 1993. Trace element geochemistry of late Palaeozoic volcanic rocks on the southern side of the Irtysh River and the evolutionary history of tectonic setting. In: Tu Guangzhi (Ed.), Progress of Solid-Earth Sciences in Northern Xinjiang, China. Beijing: Science Press, 199–216 (in Chinese with English abstract).

Miller, C.F., 1985. Are strongly peraluminous magmas derived from pelitic sediment sources? Journal of Geology, 93: 673–689.

Miller, C.F., McDowel, S.M. and Mapes, R.W., 2003. Hot and cold granites? Implications of zircon saturation temperatures and preservation of inheritance. Geology, 31: 529–532.

Misra, S.N., 1971. Chemical distinction of high-grade ortho- and para-metabasites. Norsk Geologisk Tidsskrift, 51: 311–316.

Mossakovsky, A.A., Ruzhentsev, S.V., Samygin, S.G., and Kheraskova, T.N., 1993. The Central Asian Fold Belt: geodynamic evolution and formation history. Geotectonics, 26: 455–473.

Pamic, J., Lanphere, M., and Belak, M., 1996. Hercynian I-type and S-type granitoids from the Slavonian mountains (southern Pannonian Basin, northern Croatia). Neues Jahrbuch für Mineralogie Abhandlungen, 171: 155–176.

Patiño Douce, A.E., 1997. Generation of peraluminous A-type granites by low-pressure melting of calc-alkaline granitoids. Geology, 25: 743–766.

Patiño Douce, A.E. and Harris, N., 1998. Experimental constraints on Himalayan anatexis. Journal of Petrology, 39: 689-710.

Patiño Douce, A.E., 1999. What do experiments tell us about the relative contributions of crust and mantle to the origin of granitic magmas? In: Castro, A., Fernandez, C., and Vigneresse, J.L. (Eds.), Understanding granites: integrating new and classical techniques. Geological Society of London: Special Publication, 168: 55–75.

Romer, R.L., Förster, H., and Hahne, K., 2012. Strontium isotopes- a persistent tracer for the recycling of Gondwana crust in the Variscan orogen. Gondwana Research, 22: 262–278.

Safonova, I.Y., Buslov, M.M., Iwata, K., and Kokh, D.A., 2004. Fragments of Vendian-Early Carboniferous oceanic crust of the Paleo-Asian Ocean in foldbelts of the Altai-Sayan region of Central Asia: geochemistry, biostratigraphy and structural setting. Gondwana Research, 7: 771–790.

Sajona, F.G., Maury, R.C., Bellon, H., Cotten, J., and Defant, M., 1996. High field strength element enrichment of Pliocene-Pleistocene island-arc basalts, Zamboanga Peninsula, western Mindanao (Philippines). Journal of Petrology, 37: 693–726.

Searle, M.P., Parrish, R.R., Hodges, K.V., Hurford, A., Ayres, M.W., and Whitehouse, M.J., 1997. Shisha Pangma leucogranite, south Tibetan Himalaya: field relations, geochemistry, age, origin, and emplacement. Journal of Geology, 105: 295–317.

Shan, Q., Niu, H.C., Yu, X.Y., and Zhang, H.X., 2005. Geochemistry and zircon U-Pb age of volcanic rocks from the Hanasi basin in the northern Xinjiang and their tectonic significance. Geochimica, 34(04): 315–327 (in Chinese with English abstract).

Sisson, V.B., Pavlis, T.L., and Roeske, S.M., 2003. Introduction: An overview of ridge-trench interactionin modern and ancient settings. In: Sisson, V.B.,Roeske, S.M., Pavlis, T.L. (Eds.). Geological Society of America: special paper, 371: 1–18.

Song, B., Zhang. Y.H., and Wan, Y.S., 2002. Zircon SHRIMP sample preparing, dating and discusses about related phenomena. Geology Review, 48(Suppl.): 26–30 (in Chinese with English abstract).

Song, P., Tong, Y., Wang, T., Qin, Q., Zhang, J.J., and Ning, D.X., 2017. Zircon U-Pb ages and genetic evolution of Devonian granitic rocks in the Southeastern Chinese Altai and its tectonic implications: New evidence for magmatic evolution of calc-alkaline-high K calc-alkaline-Alkaline rocks. Acta Geologica Sinica, 91(01): 55–79 (in Chinese with English abstract).

Streckeisen A. and Le Maitre R.W., 1979. A chemical approximation to the modal QAPF classification of igneous rocks. Neues Jahrbuch fur Mineralogie Abhandlungen, 136: 169–206.

Sun, M., Yuan, C., Xiao, W.J., Long, X.P., Xia, X.P., Zhao, G.C., Lin, S.F., Wu, F.Y., and Kröner, A., 2008. Zircon U-Pb and Hf isotopic study of gneissic rocks from the Chinese Altai: progressive accretionary history in the early to middle Paleozoic. Chemical Geology, 247: 352–383.

Sun, M., Long, X.P., Cai, K.D., Jiang, Y.D., Wang, B.Y., Yuan, C., Zhao, G.C., Xiao, W.J., and Wu, F.Y., 2009. Early Paleozoic ridge subduction in the Chinese Altai: Insight from the abrupt change in zircon Hf isotopic compositions. Science in China (Series D: Earth Sciences), 39(07): 935–948 (in Chinese with English abstract).

Sun, S.S. and McDonough, W.F., 1989. Chemical and isotopic systematics of oceanic basalts: implications for mantle composition and processes. Geological Society of London: Special Publication, 42: 313–345.

Sylvester, P.J., 1998. Post-collisional strongly peraluminous granites. Lithos, 45: 29–44.

Taylor, S.R., and McLennan, S.M., 1985. The continental crust: its composition and evolution. Oxford: Blackwell Publishing, 1–312.

Tong, Y., Wang, T., Hong, D.W., Liu, X.M., and Han, B.F., 2005. Zircon U-Pb age of syn-orogenic Tielieke pluton in the western part of Altay orogenic belt and its structural implications. Acta Geoscientic Sinica, 26(suppl.): 74–77 (in Chinese with English abstract).

Tong, Y., Hong, D.W., Wang, T., Wang, S.G., and Han, B.F., 2006. TIMS U-Pb zircon ages of Fuyun pos-orogenic linear granite plutons on the southern margin of Altay orogenic belt and their implications. Acta Petrologica Et Mineralogica, 25 (03): 85–89 (in Chinese with English abstract).

Tong, Y., Wang, T., Hong, D.W., Dai, Y.J., Han, B.F., and Liu, X.M., 2007. Ages and origin of the Early Devonian granites from the north part of Chinese Altai Mountains and its tectonic implications. Acta Petrologica Sinica, 23(08): 1933–1944 (in Chinese with English abstract).

Uchio, Y., Isozaki, Y., Buslov, M.M., and Maruyama, S., 2008. Occurrence of phosphatic microfossils in an Ediacaran-Cambrian mid-oceanic paleo-atoll limestone of southern Siberia. Gondwana Research, 14: 183–192.

Visonà, D., and Lombardo, B., 2002. Two-mica and tourmaline leucogranites from the Everest-Makalu region (Nepal–Tibet). Himalayan leucogranite genesis by isobaric heating? Lithos, 62: 125–150.

Visonà, D., Carosi, R., Montomoli, C., Tiepolo, M., and Peruzzo, L., 2012. Miocene andalusite leucogranite in central-east Himalaya (Everest-Masang Kang area): Low-pressure melting during heating. Lithos, 144–145: 194-208.

Wang, T., Hong, D.W., Tong, Y., Han, B.F., and Shi, Y.R., 2005. Zircon U-Pb SHRIMP age and origin of post-orogenic Lamazhao granitic pluton from Altai Orogen: its implications for vertical continental growth: Acta Petrologica Sinica, 21 (06): 640–650 (in Chinese with English abstract).

Wang, T., Hong, D.W., Jahn, B.M., Tong, Y., Wang, Y.B., Han, B.F., and Wang, X.X., 2006. Timing, Petrogenesis, and setting of Paleozoic synorogenic intrusions from the Altai mountains, Northwest China: implications for the tectonic evolution of an accretionary orogeny. The Journal of Geology, 114: 735–751.

Wang, T., Tong, Y., Jahn, B.M., Zou, T.R., Wang, Y.B., Hong, D.W., and Han, B.F., 2007. SHRIMP U-Pb zircon geochronology of the Altai No. 3 Pegmatite, NW China, and its implications for the origin and tectonic setting of the pegmatite. Ore Geology Reviews, 32: 325–336.

Wang, T., Jahn, B.M., Kovach V.P., Tong, Y., Hong, D.W., and Han, B.F., 2009. Nd-Sr isotopic mapping of the Chinese Altai and implications for continental growth in the Central Asian Orogenic Belt. Lithos, 110: 359-372.

Wang, Y.J., Yuan, C., Long, X.P., Sun, M., Xiao, W.J., Zhao, G.C., Cai, K.D., and Jiang, Y.D., 2011. Geochemistry, zircon U-Pb ages and Hf isotopes of the Paleozoic volcanic rocks in the northwestern Chinese Altai: petrogenesis and tectonic implications. Journal of Asian Earth Sciences, 42: 969–985.

Wang, J.L., Hu, Y., Wang, J.Q., and Wang, M., 2017. The Discovery of Late Ordovician Granodiorite in the Xiemisitai Area, Xinjiang and its Geological Significance. Acta Geologica Sinica (English Edition), 91 (06): 2327–2329.

Watson, E.B., and Harrison, T.M., 1983. Zircon saturation revisited: Temperature and composition effects in a variety of crustal magma Types. Earth and Planetary Science Letters, 64: 295–304.

Whalen, J.B., Currie, K.L., and Chappell, B.W., 1987. A-type granites: geochemical characteristics, discrimination and petrogenesis. Contributions to Mineralogy and Petrology, 95: 407–419.

White, A.J.R., and Chappell, B.W., 1977. Ultrametamorphism and granitoid genesis. In: Green, D.H. (ed.), Experimental petrology related to extreme metamorphism. Tectonophysics, 43: 7–22.

Windley, B.F., Kroener, A., Guo, J.H., Qu, G.S., Li, Y.Y., and Zhang, C., 2002. Neoproterozoic to Paleozoic geology of the Altai Orogen, NW China: new zircon age data and tectonic evolution. Journal of Geology, 110: 719–737.

Windley, B.F., Alexeiev, D., Xiao, W.J., Kröner, A., and Badarch, G., 2007. Tectonic models for accretion of the Central Asian Orogenic Belt. Journal of the Geological Society, London, 64: 31–47.

Williams, I.S., and Claesson, S., 1987. Isotope evidence for the Precambrian province and Caledonian metamorphism of high grade paragneiss from the Seve Nappes, Scandinavian Caledonide, II. Ion microprobe zircon U-Th-Pb. Contributions to Mineralogy Petrology, 97: 205–217.

Wright J.B. 1969. A simple alkalinity ratio and its application to questions of non-orogenic granite gneiss. Geological Magazine, 106: 370–384.

Wu, F.Y., Li, X.H., Yang, J.H., and Zheng, Y.F., 2007. Discussions on the petrogenesis of granites. Acta Petrologica Sinica, 23(6): 1217–1238 (in Chinese with English abstract).

Xiao, W.J., Windley, B.F., Badarch, G., Sun, S., and Qin, K.Z., 2004. Palaeozoic accretionary and convergent tectonics of the Southern Altaids: implications for the growth of Central Asia. Journal of the Geological Society of London, 161: 339–342.

Xiao, W.J., Han, C.M., Yuan, C., Sun, M., Lin, S.F., Chen, H.L., Li, Z.L., Li, J.L., and Sun, S., 2008. Middle Cambrian to Permian subduction-related accretionary orogenesis of Northern Xinjiang, NW China: implications for the tectonic evolution of central Asia. Journal of Asian Earth Sciences, 32: 102–117.

Xiao, W.J., Windley, B.F., Yuan, C., Sun, M., Han, C.M., Lin, S.F., Chen, H.L., Yan, Q.R., Liu, D.Y., Qin, K.Z., Li, J.L., and Sun, S., 2009. Paleozoic multiple subduction-accretion processes ofthe southern Altaids. American Journal of Science, 309: 221–270.

Xinjiang Bureau of Geology and Mineral Resources. 1978.1: 200000 regional geological reports on Altay. Unpublished (in Chinese).

Yu, X.Y., Mei, H.J., Yang, X.C., and Wang, J.D., 1993. Irtysh volcanic rocks and tectonic evolution. In: Tu Guangzhi (ed.), Progress of Solid-Earth Sciences in Northern Xinjiang, China. Beijing: Science Press, 185–198 (in Chinese with English Abstract).

Yuan, C., Sun, M., Xiao, W.j., Li, X.h., Chen, H.L., Lin, S.F., Xia, X.P., and Long, X.P., 2007. Accretionary orogenesis of the Chinese Altai: insights from Paleozoic granitoids. Chemical Geology, 242: 22–39.

Yuan, F., Zhou, T.F., and Yue, S.C., 2001. The ages and the genetic types of the granites in the Nurt Area, Altay. Xinjiang Geology, 4(12): 292–296 (in Chinese with English abstract).

Zeng, Q.S., Chen, G.H., Wang, H., and Shan, Q., 2007. Geochemical characteristic, SHRIMP ziucon U-Pb dating and tectonic implication for granitoids in Chonghuer basin, Xinjiang. Acta Petrologica Sinica, 23(08): 1921–1932 (in Chinese with English abstract).

Zhang, C., and Huang, X., 1992. The ages and tectonic setting of ophiolites in West Junggar, Xinjiang. Geology Review, 38 (06): 509–524 (in Chinese with English abstract).

Zhang, X.B., Sun, J.X., and Li, Z.C., 1996. Tectonic evolution and minerogenic series of Erqis Structural Belt. Beijing: Scientific Publishing House, 205 (in Chinese).

Zhang, Y., Xu, X.Y., Chen, J.L., Zhang, H.Y., Tang, Z., Sun, X.P., and Li, X.B., 2012. Geological characteristics and LA-ICP-MS zircon U-Pb age ofMayinebo ophiolite in Altay orogenic belt. Geological Bulletin of China, 31(06):834–842 (in Chinese with English abstract).

Zhao, Y.J., Yuan, C., Zhou, M.F., Yan, D.P., Long, X.P., and Li, J.L., 2007. Geochemistry and petrogenesis of Laojungou and Mengtougou granites in western Sichuan, China: Constrains on the nature of Songpa-Ganzi basement. Acta Petrologica Sinica, 23(05): 995–1006 (in Chinese with English abstract).

Zhu, D.C., Mo, X.X., Niu, Y.L., Zhao, Z.D., Wang, L.Q., Pan, G.T., and Wu, F.Y., 2009. Zircon U-Pb dating and in-situ Hf isotopic analysis of Permian peraluminous granite in the Lhasa terrane, southern Tibet: Implications for Permian collisional orogeny and paleogeography. Tectonophysics, 469: 48–60.

Zhu, Y.F., Zeng, Y.S., and Gu, L.B., 2006. Geochemistry of the rare metal-bearing pegmatite No. 3 vein and related granites in the Keketuohai region, Altay Mountains, northwest China. Journal of Asian Earth Sciences, 27: 61–77.

Zhu, Y.F., and Song, B., 2006. Petrology and SHRIMP chronology of mylonitized Tianger granite, Xinjiang: also about the dating on zircon hydrothermal zircon rims in granite. Acta Petrologica Sinica, 22(01): 135–144 (in Chinese with English Abstract)

About the first and corresponding author

LIU Feng, male, born in 1968 in Shihezi City, The Xinjiang Uygur Autonomous Region; doctor; graduated from China University of Geosciences in Wuhan city; researcher; Institute of Mineral Resources, Chinese Academy of Geological Sciences. He is now interested in the study on the ore deposit geochemistry. Email: liufeng@cags.ac.cn; phone: 010-68999096, 18611869922.